Sedimentary Geology xxx (2017) xxx–xxx

Contents lists available at ScienceDirect

Sedimentary Geology

journal homepage: www.elsevier.com/locate/sedgeo

Boulder emplacement and remobilisation by cyclone and submarine landslide tsunami waves near Suva City, Fiji

A.Y. Annie Lau [a,*], James P. Terry [b,c], Alan Ziegler [d], Arti Pratap [e], Daniel Harris [a]

[a] School of Earth and Environmental Sciences, The University of Queensland, Brisbane, QLD 4072, Australia [b] College of Natural and Health Sciences, Zayed University, Dubai, United Arab Emirates [c] Steering Group on Natural Hazards and Disaster Risk, International Council for Science, Regional Office for Asia and the Pacific (ICSU ROAP), Kuala Lumpur, Malaysia [d] Department of Geography, National University of Singapore, Singapore [e] School of Geography, Earth Sciences and Environment, The University of the South Pacific, Suva, Fiji

article info

Keywords:
Extreme waves
Coastal hazards
South Pacific
Tropical cyclone
Submarine landslide
Age-dating

Article history:
Received 5 March 2017
Received in revised form 8 December 2017
Accepted 14 December 2017
Available online xxxx

abstract

Kina (1993), appear to have remobilised some large boulders. While prior research has demonstrated headward retreat of Suva Canyon in response to the repeated occurrence of earthquakes over the past few millennia, our results highlight the lingering vulnerability of the Fijian coastlines to high-energy waves generated both in the presence (tsunami) and absence (storm) of submarine failures and/or earthquakes. To explain the age discrepancies of U-Th dated coral comprising the deposited boulders, we introduce a conceptual model showing the role of repeated episodes of tsunamigenic submarine landslides in removing reef front sections through collapse. Subsequent high-energy wave events transport boulders from exposed older sections of the reef front onto the reef where they are deposited as 'new' boulders, alongside freshly detached sections of the living reef. In similar situations where anachronistic deposits complicate the deposition signal, age-dating of the coral boulders should not be used as a proxy for determining the timing of the submarine landslides or the tsunamis that generated them.

The characteristics of a reef-top boulder field created by a local submarine landslide tsunami are presented for the first time. Our examination of large reef-derived boulders deposited by the 1953 tsunami near Suva City, Fiji, revealed that shorter-than-normal-period tsunami waves generated by submarine landslides can create a boulder field resembling a storm boulder field due to relatively short boulder transport distances. The boulder-inferred 1953 tsunami flow velocity is estimated at over 9 m s^{-1} at the reef edge. Subsequent events, for example Cyclone

1. Introduction

Coastal boulders transported by high-energy wave (HEW) events, such as storms and tsunamis, have been studied at various locations worldwide for approximating the magnitude and occurrences of past extreme wave events (e.g., Noormets et al., 2004; Hall et al., 2006; Scicchitano et al., 2007; Goto et al., 2010; Engel and May 2012; Salzmann and Green, 2012; Yu et al., 2012; Araoka et al., 2013; ShahHosseini et al., 2016; Terry et al., 2016). New boulders deposited in modern storms and tsunamis have been described in detail (e.g., 1951–2004 Okinawa typhoons: Goto et al., 2011; 2004 Indian Ocean tsunami: Goto et al., 2007; 2009 South Pacific tsunami: Etienne et al., 2011; 2010 Chile tsunami: Spiske and Bahlburg, 2011; 2011 Tohoku-oki tsunami: Yamada et al., 2014; 2013 Typhoon Haiyan: May et al., 2015; Kennedy et al., 2017; Soria et al., 2017; 2016 Cyclone Winston: Terry and Lau, 2018). However, there remains a lack of research on boulder fields that resulted from landslide tsunamis. Herein, we present a case study from Fiji where large carbonate boulders were primarily dislodged and deposited by a local submarine landslide tsunami that occurred in 1953.

On 14 September 1953, a M_w6.75 earthquake was generated by the rupture of a 30-km strike-dip fault segment S of the coast of Viti Levu Island in Fiji (Houtz, 1962; Rahiman et al., 2007) (Fig. 1). Although of moderate magnitude, the earthquake induced a tsunamigenic submarine landslide and associated collapse of a seaward-facing section of fringing coral reefs. Tsunami waves

* Corresponding author.
E-mail address: annie.lau@uq.edu.au (A.Y.A. Lau).

https://doi.org/10.1016/j.sedgeo.2017.12.017 0037-0738/

struck Suva, the capital city, within a few minutes, inundating low-lying areas, killing five people. On Namuka and Lami Reefs (hereafter called NL (Namuka-Lami) Reefs; 18°8.700′S, 178°22.900′E), which fringe the coastline immediately W of Suva, more than a hundred isolated large carbonate boulders are clustered around the opening of Rat-tail Passage that separates Namuka and Lami Reefs (Fig. 2). Most of these boulders were reported by eyewitnesses to have been cast up by the 1953 tsunami (The Fiji Times & Herald, 1953a; Houtz, 1962; Atkinson and Collen, 2000; Rahiman, 2006; Collen et al., 2011).

2. Study area

2.1. Historical accounts of the 1953 tsunami and boulder transport

At 12:26 pm Fiji standard time on 14 September 1953, b10 s after the M_w6.75 earthquake was felt in Suva, eyewitnesses observed a drop in sea level at the entrance to Suva Harbour. Some observed "a large brown "bubble" had arisen between the entrance beacons, and the first annular wave from this disturbance had struck the reef" (Houtz, 1962, p.7). The first and largest tsunami wave arrived at the western shore of Suva Peninsula 3–4 min afterwards. Eyewitnesses reported the wave reached 3–15 m in height when it broke at the reefs at Suva harbour and along the southern coast (Houtz, 1962). Measured maximum wave heights were N3 m and run-up heights reached 2 m (Prasad et al., 2000; Rahiman et al., 2007). A photo taken at the time showed a 1.5–2.0 m high bore crest. The inundation distance at the southern tip of the Suva Peninsula was estimated from a boat carried over 100 m inland (Rahiman et al., 2007). About 4 km W of Suva, eyewitnesses at Muaivuso village (18°8.400′S, 178°21.600′E) behind NL Reefs

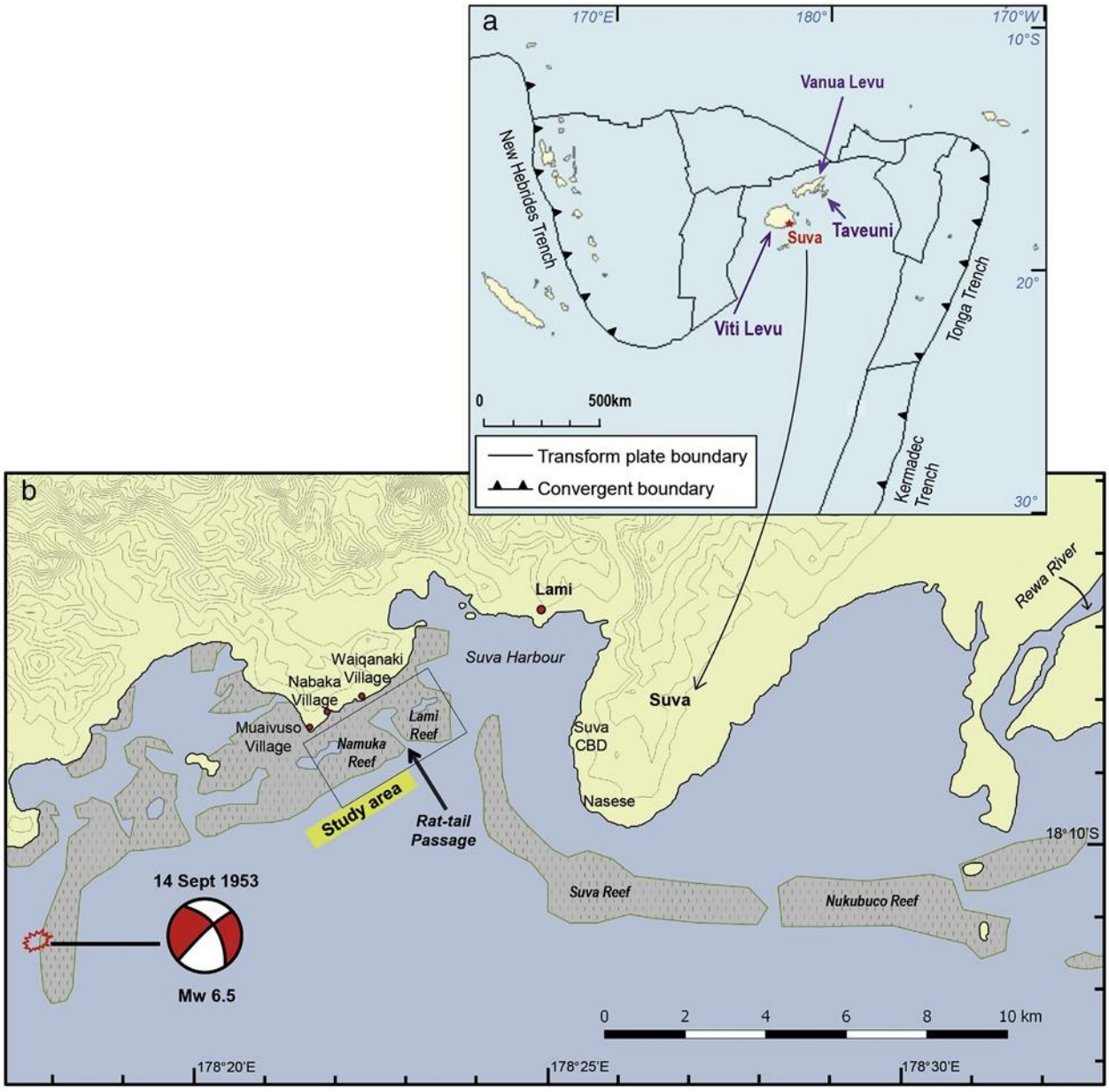

Fig. 1. Regional setting and location of the study site. (a) Plate boundaries surrounding Fiji. The labelled submarine trenches are the major subduction zones in the region. (b) Locations of the study area, the 1953 earthquake epicentre and focal mechanism (Hamburger et al., 1990), and other places mentioned in the text. Land elevation contours are at 20 m intervals.

Despite being mentioned multiple times by the media and the academic literature, this boulder field has not been studied in detail. The aims of this study are to (1) provide detailed information on the characteristics and distribution of boulders formed by the 1953 local submarine landslide tsunami; (2) investigate post-1953 boulder remobilisation and reef morphology at the study site for improving understanding of coastal hazard characteristics in Suva and the surrounding urban area, a major economic hub in the South Pacific Islands; and (3) reveal specific challenges in reconstructing long-term tsunami history on a submarine-landslide-prone reef.

described a 3 m high wall of muddy water sweeping across the reef flat, hitting the low cliffs in front of the village. The tsunami source was identified as a 60 million m^3 submarine landslide off Lami Reef (Rahiman et al., 2007) (Fig. 3a). An aerial photo taken 12 days later showed that 30–50 m of reef scarp was missing, indicating a part of the canyon wall had slipped into the sea following the earthquake.

Please cite this article as: Lau, A.Y.A., et al., Boulder emplacement and remobilisation by cyclone and submarine landslide tsunami waves near Suva City, Fiji, Sedimentary Geology (2017), https://doi.org/10.1016/j.sedgeo.2017.12.017

Fig. 2. Large boulders on Namuka-Lami Reefs investigated in this study. (a) Clusters of boulders on the reef crests. Suva city is in the background, approximately 4 km behind the boulder field. The direction of view is indicated in Fig. 3. (b) Closer view of two large boulders (LR209: 23.7 m^3 and LR210: 26.2 m^3); (c) a tall-standing, 18.1 m^3 boulder (NR150); (d) close up of a typical carbonate boulder studied (LR234). The boulder lithology is boundstone. Boulders are typically encrusted by intertidal organisms: 1- barnacles (Tetraclita squamosa viridis), 2patterns of chiton grazing, 3- eroded fossil coral (Acropora sp.?); (e) A 1.2 m^3 overturned fossil table coral in the back-reef area behind the Muaivuso Lagoon.

Villagers in Muaivuso recalled that large boulders appeared at the time of the tsunami (Houtz, 1962; Atkinson and Collen, 2000; Collen et al., 2011). Newspaper articles similarly described previously unseen boulders, as well as older, pre-1953 boulders that had been identified on reef flats earlier by the Geological Survey of Fiji (The Fiji Times & Herald, 1953a, 1953b). Rahiman (2006) described the 1953 tsunami boulders as large ("from 20 to 30 cubic metres", p.133) and close to the reef edge near Rat-tail Passage, whereas older, weathered and smaller boulders were found behind the landward limit of the 1953 boulders. By comparing the modern locations of boulders to those visible on a 1951 aerial photo, Rahiman (2006) specified that older boulders had apparently shifted 200 m landward, plausibly during the 1953 tsunami. More recently, villagers have reported that some smaller boulders of b2 m^3 had been remobilised by tropical cyclones after the tsunami (Atkinson and Collen, 2000).

2.2. Tectonic setting and other tsunami sources

The risk of earthquakes and tsunamis in Fiji has been studied extensively since the 1953 tsunami (e.g., Prasad et al., 2000; SPDRP, 2002; Rahiman, 2006; Pearce, 2008). The Fiji Islands lie within a relatively complex tectonic setting. To the W and E respectively, tectonic activity in the New Hebrides Trench and the Tonga-Kermadec Trench is capable of generating regional tsunamis that can reach Fiji within 1 to 2 h (Pearce, 2008) (Fig. 1). Prehistorically, a local legend possibly passed down from 400 to 500 years ago, described the arrival of great waves at the mouth of Rewa River that flooded valleys for many miles (Reed and Hames, 1967) (see Fig. 1 for the location of Rewa River). This phenomenon was inferred to be a tsunami event. Historically since 1868, 33 tsunamis have affected Fiji, although most have been minor events with b0.5 m of water fluctuation (NOAA historical tsunami database, 2016). In 1976 and 1999, run-up heights of 0.9 and 1.0 m were measured at Suva following earthquakes at the Tonga-Kermadec and New Hebrides Trenches, respectively (Pearce, 2008). Pacific-wide, Thomas et al. (2007) proposed that any M_w9.0 earthquake at major subduction zones could

Please cite this article as: Lau, A.Y.A., et al., Boulder emplacement and remobilisation by cyclone and submarine landslide tsunami waves near Suva City, Fiji, Sedimentary Geology (2017), https://doi.org/10.1016/j.sedgeo.2017.12.017

generate a tsunami with an offshore deep-water amplitude of over 0.75 m in Fiji. For comparison, the maximum amplitude of the 2004 Indian Ocean tsunami was estimated at only 0.6 m in the open ocean, but resulted in run-up heights of tens of metres at affected coasts in Indonesia (Song et al., 2005).

Near Suva, a series of strike-slip faults exist in SE Viti Levu (Rahiman and Pettinga, 2006). Fortunately, because of the complexity of the interlocking fault sets, the rupture of a single fault is rarely of sufficient length to produce a large earthquake. In the last 150 years, there has been only one earthquake $NM_w6.0$, that in 1953. The maximum possible magnitude of an earthquake in SE Viti Levu is assessed at $M_w7.0–7.5$, the recurrence interval of a $M_w6.0–7.0$ earthquake is estimated at 1300– 1500 years (±500 years) – however this estimation is based on limited available data, hence these values "should be used with caution" (SPDRP, 2002, p.13). Rahiman and Pettinga (2006) used an empirical model to estimate that the collapse of the Suva Canyon head might be capable of generating a tsunami with initial amplitude up to 16 m following a local earthquake, in a worst-case scenario.

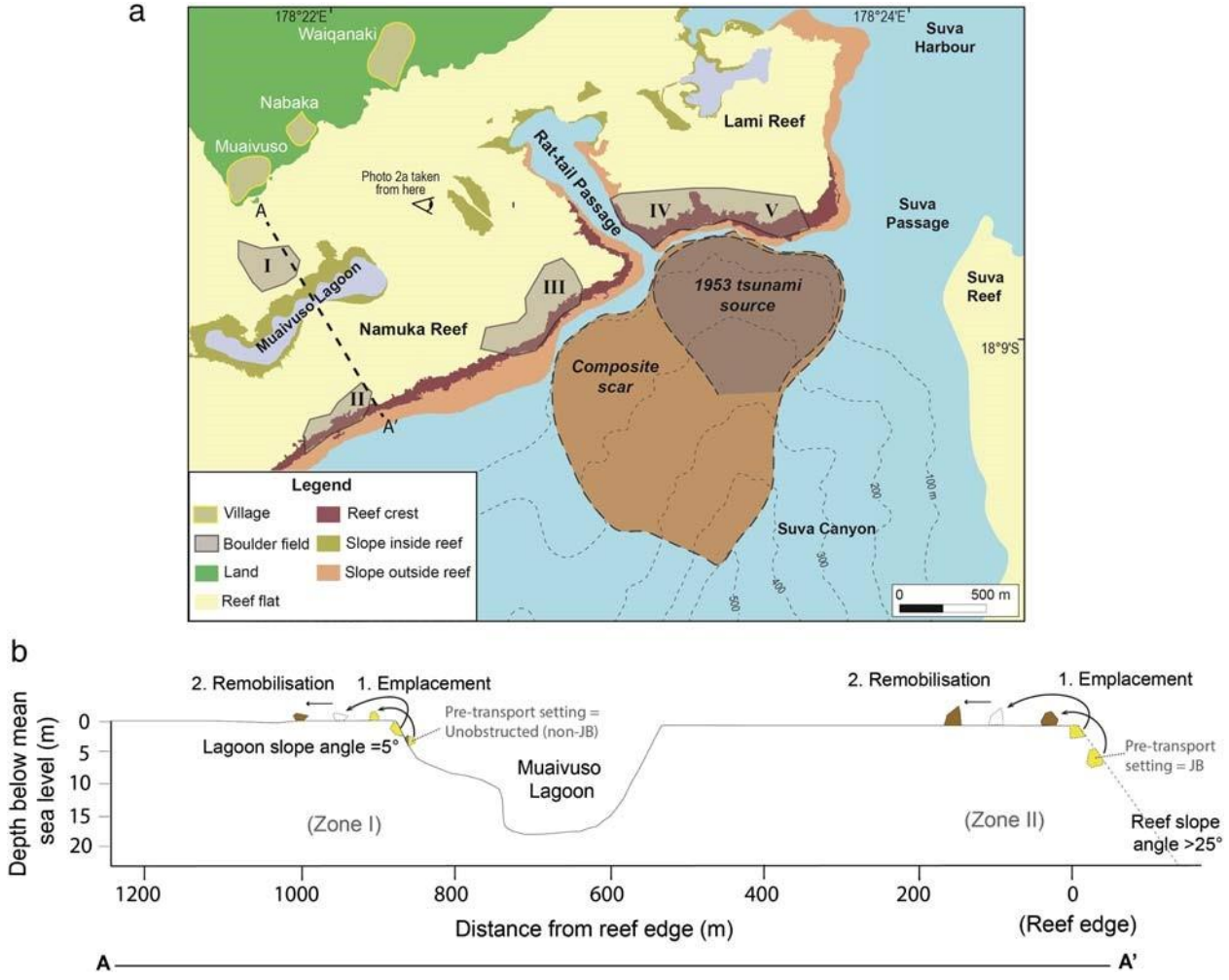

Fig. 3. (a) Map illustrating the 1953 tsunamigenic submarine slope failure and its contribution to a larger composite landslide scar that exists offshore at the head of the submarine Suva Canyon. Landslide scars and bathymetry are redrawn from Rahiman (2006). The boulder fields examined on NL Reefs are separated into five zones (I to V) for analyses, according to location and local shore orientation. Reef geomorphic features on NL Reefs are based on data from Roelfsema and Phinn (2008). (b) Bathymetric profile for A-A′ on Namuka Reef is adapted from Atkinson and Collen (2000). Boulder emplacement and remobilisation are also illustrated on the profile. Boulders on the profile are not drawn to scale. JB stands for joint-bounded.

2.3. Coastal setting

The Namuka-Lami Reefs are a near-continuous formation of fringing coral reefs that extend ENE to WSW along the coastline NW of Suva Harbour. The seaward margins of the Namuka and Lami Reefs are about 7 and 1.5 km long, respectively, separated by the NW-trending, 20–30 m deep, T-shaped Rat-tail Passage (Atkinson and Collen, 2000). At their landward extent, the NL Reefs merge into mangrove forests at the low-lying shoreline. Behind the mangroves are low headlands on which several Fijian villages are situated at approximately 5 m elevation. Although the southern part of Viti Levu was uplifted during the Holocene, and sea level reached a maximum of 2.1 m above present sea level around 4200 BP (Nunn and Peltier, 2001), a small portion of the local marl bedrock b0.8 m high situated close to Muaivuso Village is the only emerged feature on NL Reefs, besides wave-deposited boulders. The reef flats extend 1.5–2.0 km seawards from the shoreline, and are dominantly covered by sand (Roelfsema and Phinn, 2008). A series of elongated lagoons, including the 28 m deep Muaivuso Lagoon, occupy the back-reef zone. Closer to the reef edge, the reef crest is approximately 40 to 130 m wide, as mapped using multi-scale image analysis (Phinn et al., 2012) (Fig. 3a). The outermost part of the crest is raised a few cm into a gentle convex arc (Atkinson and Collen, 2000). The seaward edge of NL Reefs forms the headward margin of an offshore submarine canyon called the Suva Canyon. Here, a composite submarine landslide scar has been identified, indicating the canyon head had failed multiple times in the past (Rahiman, 2006). The repeated failure of the canyon head is a result of the steep slope angle (25°) and high sedimentation rates contributed by terrestrial sediments discharging from the Rewa River (Rahiman, 2006).

2.4. Wave climate

Suva has a tidal range of up to 2 m (Australian Government Bureau of Meteorology (BoM), 2015). The sea completely submerges the reefs, except during low spring tides when they are exposed by a few cm above sea level. Under calm conditions, tidal currents are ≤0.51 m s^{-1} (Atkinson and Collen, 2000). The prevailing SE trade winds, strongest in the cool dry season from May to October, drive swells in directions generally perpendicular to the reef front (Fiji Meteorological Service (FMS), 2006; Singh and Aung, 2008). For Suva, mean wave height and period are 0.88 m and 12.63 s, respectively; 99% of wind-driven waves are Þ2.9 m in height, while the largest 10% of the waves over 1.74 m predominantly come from the SE (130–170°) (Bosserelle et al., 2015). The 1 in 50 year maximum wind-driven wave height is estimated to be 7.8 m (BoM and CSIRO, 2014).

The tropical cyclone season in Fiji usually spans November to April during the hot rainy summer. Two or three tropical cyclones cause severe damage to Fiji each decade (FMS, 2001, 2006). For Viti Levu Island, the NW coast is more frequently affected than the SE coast, where Suva is located, because tropical cyclone track directions from the N and W towards the island are most typical (Terry, 2007; Terry and Gienko, 2010). From 1969 to 2010, only 93 tropical cyclones crossed within 500 km of Suva, an average of 2.2 per season (Southern Hemisphere Tropical Cyclone Data Portal, 2011).

3. Methods

3.1. Boulder data collection

3.1.1. Field measurements and mapping

Fieldwork was carried out on the NL Reefs at times of low spring tide over four days in September 2013. The following features of each boulder were recorded directly in the study area: location coordinates, 3D shape (i.e., rectangular prism, triangular prism, ellipsoidal or irregular) and dimensions (i.e., maximum lengths along long (a-), intermediate (b-) and short (c-) axes). As water flow normally rotates a boulder's a-axis to a flow-perpendicular alignment (Imamura et al., 2008; Nandasena and Tanaka, 2013), the long axis orientation for boulders with an a-axis that was 20% or more longer than the b-axis was used to interpret wave direction. All visible boulders with an a-axis over 1 m were measured, although it is likely that shorter clasts were missed if they were fully submerged before or after the lowest tide level. The perpendicular distance of boulders to the nearest reef edge, as delimited from the 2013 satellite image on Google Earth, was measured using the Esri ArcMap software. Boulders situated in a back-reef area behind Muaivuso Lagoon were also included in the dataset (Fig. 3).

Closer to the Lami Reef edge, at least 18 small boulders were observed in an approximately 5800 m^2 area (roughly 120 m wide and 50 m long). Owing to their short vertical heights, the time of their emergence at low tide was limited. Instead of measuring these clasts individually, the extent of this area was mapped with a GPS, and the number of small boulders was counted in the field. We measured three boulders in this group to estimate volumes of all small boulders present within this area (one example measured 1.3 × 1 × 0.45 m). During data analysis, the extent of this area was drawn on the map. The locations of 18 boulders with similar dimensions to the representatives were added randomly within this area for further analyses, together with all other measured boulders.

3.1.2. Boulder volume, form, and density determination

Volumes were calculated for boulders with regular geometric shapes by simple geometric formulae for rectangular prism, triangular prism, and ellipsoid. For rectangular boulders, estimated volumes were multiplied by a scaling factor of 0.7, an adjustment needed to lessen the problem of volume overestimation that has been highlighted in earlier studies (Engel and May 2012; Scicchitano et al., 2012; Gienko and Terry, 2014; Lau et al., 2016). Some clasts were highly weathered, exhibiting irregular shapes that cannot be simply categorised as rectangular, triangular, or ellipsoidal. Volumetric determinations for such boulders were based on their own unique shapes, using the closest combination of standard geometries.

The flatness index (FI) – sometimes referred to as the Cailleux Flatness Index – of each boulder was determined as FI = (a + b)/2c. The index ranges from 1 to ∞, with a value near 1 indicating that all axes are of similar length, meaning the clast is "equant" in form. Clasts with a high FI above 3 are extremely "non-equant": i.e., platy, flat, or elongated (Wentworth, 1922; Cailleux, 1945; Blott and Pye, 2008).

A mean boulder density of 1.3 g cm^{-3} was determined based on samples chiselled from six boulders showing lower levels of postdepositional weathering, as they better resemble the clast condition at the time of transport. Sample bulk density (BD) was calculated based on the eq. BD = M_a/ BV, where M_a and BV are dry mass and bulk volume of sample, respectively. The dry mass of samples was measured on a digital balance (accuracy to 0.01 g). Bulk volume was determined via water displacement, whereby a plastic-wrapped sample was lowered into a water-filled beaker and the difference in water level was recorded as sample volume.

3.1.3. Boulder age-dating

Rock samples were chiselled from the youngest surfaces of six boulders for laboratory density measurement and Uranium-Thorium (U-Th) dating. Age-dating was carried out in an attempt to corroborate the timing of coral mortality with the 1953 tsunami that quarried the living reef framework and transported the boulders on top of the reef flats. The underpinning assumption is that living and growing corals were dislodged from the submerged reef slope and emplaced onto the reef flat by extreme tsunami waves before they subsequently died (Yu et al., 2009; Terry and Etienne, 2014). This phenomenon was originally believed to have occurred on NL Reefs because "live/dead corals" were mapped on the reef slope (Roelfsema and Phinn, 2008), and fragments of freshly broken corals (Acropora valida) were observed on the reef crest, indicating the presence of living corals on the reef slope.

The principle of U-Th dating is that ^{238}U decays to stable ^{206}Pb via a series of daughter isotopes, including ^{234}U and its daughter isotope ^{230}Th. If a uranium mineral is left undisturbed in a closed system for several million years, secular equilibrium will be reached when the rate of decay (i.e., the activity) of each daughter isotope equals that of the parent isotope (Walker, 2005). In an aqueous system, growing hermatypic corals take up small amounts of soluble uranium from seawater and incorporate the element into their carbonate skeleton, whereas thorium, being insoluble, is not present. Once the carbonate has been formed the system becomes closed. A state of disequilibrium in the activities of ^{238}U, ^{234}U and ^{230}Th remains for approximately 500,000 years (about seven times the half-life of ^{230}Th) before secular equilibrium is reached (Smart, 1991; Walker, 2005; Zhao et al., 2009). As the system approaches equilibrium at a predictable rate, the time since carbonate formation can be calculated by measuring the parent-daughter ratio if the initial state of the system is known.

The ages of carbonate samples were determined by measuring the $^{230}Th/^{238}U$ and $^{234}U/^{238}U$ ratios via multi-collector inductively coupled plasma mass spectrometry (MC-ICP-MS) at the Radiogenic Isotope Facility of the University of Queensland, and applying the following equation (Zhao et al., 2009, modified after Edwards et al., 1987):

$$1-\frac{^{230}Th}{^{238}U} = e^{-\lambda_{230}T}-\frac{^{234}U}{^{238}U}\left(1-\frac{\lambda_{230}}{\lambda_{230}-\lambda_{234}}\left(1-e^{(\lambda_{234}-\lambda_{230})T}\right)\right) \quad (1)$$

where T is the age of the sample, λ_{230} is the decay constant of ^{230}Th = (9.158 ± 0.028) × 10^{-6} $year^{-1}$, and λ_{234} is the decay constant of ^{234}U = (2.8262 ± 0.0057) × 10^{-6} $year^{-1}$ (decay constants following Cheng et al., 2000). Details of the laboratory procedures for age-dating are provided in Clark et al. (2014a, 2014b) and Liu et al. (2016).

3.2. Historical aerial photos and satellite images

Aerial photos and satellite images were used to determine changes in reef-edge outline and boulder positions on NL Reefs over recent decades. Four aerial photos were provided by the Fiji Department of Lands and Surveys for the years 1954, 1978, 1986 and 1994. The photos were taken from altitudes of 20,000 ft. (6100 m), 11,000 ft. (3400 m), 26,000 ft. (7900 m) and 25,000 ft. (7600 m), respectively. Unfortunately, the 1951 aerial photo examined by Rahiman (2006) or other pre-1953 photos could not be obtained to verify the transport of preexisting boulders by the 1953 tsunami (Department of Lands and Surveys, Fiji, Personal Communication). Satellite images spanning 2005 to 2016 were examined on Google Earth. The earliest image with a sufficiently fine resolution to show the presence of larger boulders on the studied reefs was dated January 2005 (Google Earth, 2005). Boulders on aerial photos were identified by comparing their shapes and sizes to actual boulder measurements. The a- and b-axes of boulders on images were measured with the measuring line tool after aerial photos were geo-referenced and imported for display into QGIS software (QGIS Development Team, 2013).

3.3. Flow velocity estimations

We back-calculated the minimum flow velocity (MFV) required to initiate movement of each boulder using the hydrodynamic equations proposed by Nandasena et al. (2011) to estimate the power of past tsunami and storm waves. The equations assume boulders were already detached from the reef prior to movement, and that they were sitting in one of the two pre-transport settings — either on an unobstructed surface or in a joint-bounded socket. Boulders on an unobstructed surface could be moved by sliding, rolling, or lifting (Nandasena et al., 2011):

$$u^2 \geq \frac{2(\rho_s/\rho_w - 1)gc\cos\theta}{C_l} \quad \text{(Lifting)} \quad (4)$$

while movement of joint-bounded boulders could only be initiated if the lift force alone was sufficient to dislodge the boulders:

$$u^2 \geq \frac{2(\rho_s/\rho_w - 1)gc\cos\theta\,\mu_s \sin\theta}{C_l} \quad \text{(Lifting)} \quad (5)$$

In all equations, u is flow velocity (m s^{-1}); b and c are the boulder intermediate and short axes respectively (m); ρ_s is boulder density (g cm^{-3}); ρ_w is seawater density (1.02 g ml^{-1}); C_d is the drag coefficient (1.95); C_l is the lift coefficient (0.178); θ is the angle of the bed slope at pre-transport location (°); μ_s is the coefficient of static friction (0.5); and g is gravitational acceleration (9.81 m s^{-2}).

In this study, the MFVs for boulder emplacement and remobilisation were calculated separately. For boulder emplacement, i.e., when a part of the reef is dislodged by a wave and thrown onto the reef flat, Eq. (5) was used. This is because no remnants of emerged old reef and other boulder source were present on NL Reefs, implying these boulders were sourced from the submarine reef framework. A pre-transport bed slope angle of 25° was conservatively selected as it was determined as the "pre-failure slope angle" of the Suva Canyon landslide (Rahiman, 2006). The slope angle at the lagoon edge is determined as 5° from a cross-sectional profile in the work of Atkinson and Collen (2000). Due to the gentle slope angle at the lagoon edge, it is possible that coral

Table 1

heads were emplaced onto the subaerial reef flat from an unobstructed lagoon floor (Fig. 3b). Estimations from Eqs. (2)–(4) were therefore also used to determine the MFVs to emplace zone I boulders.

For boulder remobilisation, Eqs. (2)–(4) were used as the boulders were already sitting on top of the reef flat. They could potentially be remobilised by all three transport modes. The bed slope angle in this scenario is taken as 0° because NL Reef flats are not inclined.

3.4. Storm wave modelling

Storm wave conditions on the reef flats for zones I and II were modelled using a 1D phase resolving non-hydrostatic model (XBeach Kingsday Release in Non-Hydrostatic Mode, Roelvink et al., 2015). This model calculated the transformation of deep water storm waves to reef flat current flow using a range of offshore wave conditions. The likely sea state of each storm event based on offshore significant wave height (H_{so}) and period were generated using a JONSWAP spectrum over 17 min with an enhancement factor of 3.3 (Buckley et al., 2014). A wave friction factor (a function of the relative bed roughness under waves (Nielsen, 1992)) of 0.3, which is comparable to a moderately rough reef (Monismith et al., 2013; Baldock et al., 2014), was also used to include the high frictional wave energy dissipation observed on coral reefs (e.g., Rogers et al., 2016). All other free parameters were set at default values. Successive runs of the model were performed from H_{so} = 0.5 m to H_{so} = 9.5 m at intervals of H_{so} = 0.5 m. The wave period for each run was kept constant at 12 s, which is based on Bosserelle et al. (2015), who reported that wave periods of approximately 10–12 s were associated with the largest storm events in the historical wave record.

The models were run at high tide with a storm surge of 1 m based on storm surge analysis for the port of Suva, Fiji. A 1 m storm surge was determined to be a 1 in 30 year event (Carter et al., 1991) and was comparable to the wave event (H_{so} = 6.27 m) reported in 1993, which was also determined to be a 1 in 30 year event (Bosserelle et al., 2015). The maximum Eularian current velocity (u (m s^{-1})) was determined in zones I and II for each of the model runs from H_{so} = 0.5 m to H_{so} = 9.5 m. This velocity represents the maximum current flow generated by waves in zones I and II during the model runs. The current flow determined from the wave model is comparable to the velocities required to transport the boulders determined by the Nandasena et al. (2011) equations. The potential offshore wave conditions required to transport the boulders by sliding (minimum velocity required for remobilisation) and lifting (for emplacement) in zones I and II could then be determined.

4. Results

4.1. Boulder characteristics

A total of 136 boulders were examined in this study. Boulders are comprised of coral fabric originally derived from the reef framework and are identified as boundstone, a type of calcareous rock where components have been bound together after deposition (Dunham, 1962). Coral species that

made up these boulders are, however, rarely identifiable due to post-depositional weathering. No boulders of other

U-Th ages of six large boulders around Rat-tail Passage on Namuka and Lami Reefs. All errors are quoted as 2σ.

Boulder	Boulder volume (m^3), mass (t)	U (ppm)	^{232}Th (ppb)	(^{230}Th/^{232}Th)	(^{230}Th/^{238}U)	(^{234}U/^{238}U)	Corrected age (year)	Mortality year
NR150	18.1 m^3, 23.6 t	2.6634 ± 0.0010	0.2426 ± 0.0005	1711.91 ± 6.16	0.05140 ± 0.00015	1.1462 ± 0.0009	4996 ± 16	2982 ± 16 BCE
LR227	25.3 m^3, 32.9 t	3.6822 ± 0.0035	0.5433 ± 0.0073	941.03 ± 12.83	0.04576 ± 0.00013	1.1470 ± 0.0010	4432 ± 14	2418 ± 14 BCE
LR208	17.3 m^3, 22.5 t	2.3311 ± 0.0014	0.4462 ± 0.0009	669.92 ± 2.45	0.04226 ± 0.00013	1.1445 ± 0.0011	4095 ± 14	2081 ± 14 BCE
LR217	28.0 m^3, 36.4 t	2.6720 ± 0.0011	0.1171 ± 0.0005	2548.54 ± 14.97	0.03682 ± 0.00014	1.1446 ± 0.0010	3562 ± 14	1547 ± 14 BCE
NR158	23.8 m^3, 31.0 t	2.5199 ± 0.0012	0.0716 ± 0.0004	3374.21 ± 23.08	0.03160 ± 0.00011	1.1465 ± 0.0013	3045 ± 11	1031 ± 11 BCE
LR182	31.2 m^3, 40.5 t	3.1911 ± 0.0016	0.4368 ± 0.0008	604.81 ± 2.43	0.02729 ± 0.00010	1.1480 ± 0.0010	2618 ± 10	604 ± 10 BCE

Please cite this article as: Lau, A.Y.A., et al., Boulder emplacement and remobilisation by cyclone and submarine landslide tsunami waves near Suva City, Fiji, Sedimentary Geology (2017), https://doi.org/10.1016/j.sedgeo.2017.12.017

Table 2

Boulder count, orientation, and physical dimensions within five separate zones on NL Reefs.

Zone	I	II	III	IV	V
Number of boulders measured	16	7	34	27	34+18[a]
Mean boulder volume ± standard deviation (m^3)	1.25 ± 0.76	0.98 ± 1.17	5.85 ± 6.54	7.88 ± 6.90	3.78 ± 6.36
Median boulder volume ± median absolute deviation (m^3)	1.20 ± 0.46	0.41 ± 0.20	3.38 ± 1.84	6.08 ± 2.03	1.70 ± 1.28
Number of boulders in orientation analysis (a-axis at least 20% longer than b-axis)	10	3	32	20	28
Reef-front orientation[b]	60°–65°	60°–65°	45°–60°	70°	80°–110°
Major boulder orientation[b]	0°–20° and 80°–100°	20°–80°	40°–80°	40°–80°	80°–100°
Boulder orientation relative to shore orientation[c]	Sub-parallel to others	Parallel to sub-parallel	Parallel to sub-parallel	Parallel to sub-parallel	Parallel

[a] Volumes of 18 smaller boulders were estimated from measurements of three individual clasts (see Section 3.1.1).

[b] The degree of orientation is presented such that 0° (north) represents a N-S trend in the boulder long axis or shore orientation.

[c] The description for boulder orientation relative to the nearest reef-front is organised according to the method of Watt et al. (2010). Boulder orientation within ±10° of reef-front orientation is considered 'parallel', ±30° to reef-front is 'sub-parallel'; similarly, boulder orientation within ±10° of reef-front normal direction is 'normal', and ±30° to reef-front normal is 'sub-normal'. Other orientations are described as 'oblique' in the text.

lithologies were found on NL Reefs because the local bedrock of the Suva Marl formation is composed of calcareous siltstone and fine sandstone, which are too soft to form large, durable boulders able to withstand prolonged wave action and weathering in the coastal zone. The mean density of boulders is 1.3 ± 0.2 g cm^{-3}, based on six samples. This low density value is comparable to the 1.4 g cm^{-3} boulder density on Taveuni, Fiji, as measured by Etienne and Terry (2012), and 1.1–1.4 g cm^{-3} coral clast density among Indian Ocean tsunami boulders as presented by Paris et al. (2009). Boulder volume and mass range from a minimum of 0.21 m^3 and 0.28 t (metric tonnes) for the smallest measured clast with dimensions of 0.93 × 0.60 × 0.55 m, to 31.15 m^3 and 40.50 t for the largest individual with dimensions 7.00 × 3.74 × 2.38 m (triangular clast). Median volume and mass are 2.38 m^3 and 3.09 t, respectively.

Surface samples collected from six of the largest (N17 m^3) boulders in zones III–V date to the mid-to-late Holocene, 5000–2600 years before present (BP) based on the U-Th method. The calendar ages are 2982 ± 16, 2418 ± 14, 2081 ± 14, 1547 ± 14, 1031 ± 11, and 604 ± 10 BCE (Table 1).

4.2. Boulder distributions

The boulders are sub-divided into five spatial zones (I to V), designated according to location and local orientation of the reef edge (Fig. 3). The majority of boulders, including the largest clasts, fall into zones III, IV and V (Table 2), which are the reef-front proximal zones closest to Rat-tail Passage. Boulders in zones II to V are scattered at distances ranging from 14 to 232 m from the reef edge (i.e., from the presumed boulder source) and display a landward-fining trend (Fig. 4). In zone I, which is the most landward zone, the largest boulder (3.1 m^3) rests 945 m from the reef edge. Smaller boulders are situated farther landward.

The flatness index (FI) of boulders ranges from 1.14 (high equancy) to 6.76 (low equancy, i.e., "flat"), and is b3 for 80% of boulders on NL Reefs. Flatter boulders with FI N 3 were generally clustered closer to the reef edge. For zones II to V, almost all flat boulders (16 of 17) are located at relatively short distances (b150 m) from the reef edge (Fig. 4). Boulder flatness and distance from reef edge are weakly negatively correlated (Pearson correlation index I = −0.23, p-value = 0.02). In zone I, flat boulders (4 of 5) are located within 100 m of the landward perimeter of Muaivuso Lagoon.

Most boulders in zones II–V are orientated parallel or sub-parallel to the reef edge, whereas boulders in zone I have a bimodal pattern whereby boulders are oriented predominantly sub-parallel or oblique to the reef edge (Fig. 5). The ENE–WSW orientations of boulders in zones III and IV are comparable, despite being separated by Rat-tail Passage, while zone V differs slightly with a greater tendency for E–W orientation.

4.3. Evidence for post-1953 boulder remobilisation

Aerial photographs for years 1954, 1978, 1986 and 1994 were examined to infer whether boulder movement has occurred on NL Reefs after the 1953 tsunami. Differing resolutions and heights of aerial photography limit our ability to pinpoint boulder locations accurately for all time steps (see Supplementary Data file). As no boulders are visible in the 1954 image due to the poor image quality, this image is used only

Please cite this article as: Lau, A.Y.A., et al., Boulder emplacement and remobilisation by cyclone and submarine landslide tsunami waves near Suva City, Fiji, Sedimentary Geology (2017), https://doi.org/10.1016/j.sedgeo.2017.12.017

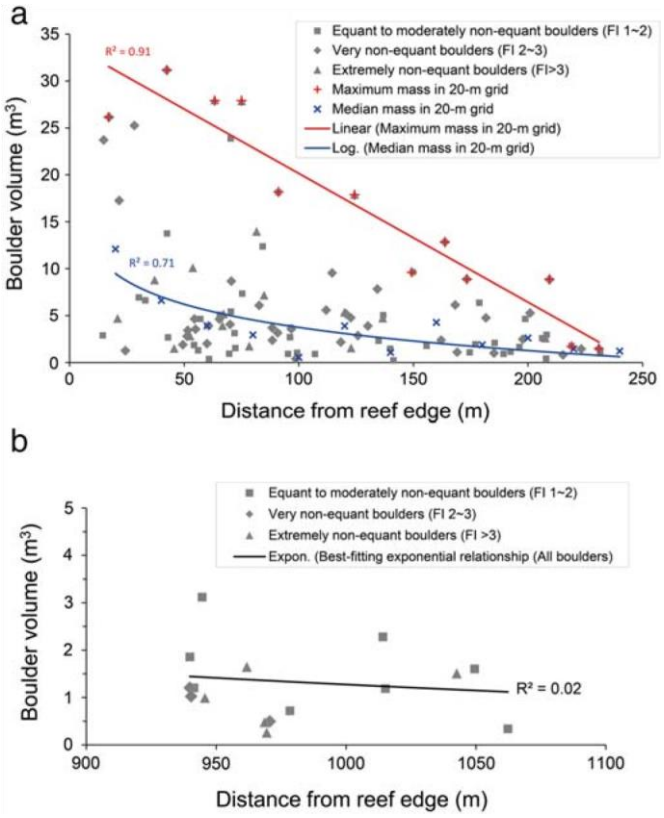

Fig. 4. Distribution of boulders of different mass and equancy of form (according to flatness index, FI), plotted relative to the seaward reef margin of NL Reefs. (a) Boulder field zones II to V are located close to the reef edge (see Fig. 3). A plot of maximum boulder mass in each 20 m grid along a transect running landward from the reef edge shows a strongly negative linear association (red line). Median boulder mass in the same 20 m grids also diminishes landward, demonstrating a moderately-strong negative logarithmic relationship (blue line). (b) The boulder field of zone I is displayed with reference to the reef edge to show the landward-fining trend. (For interpretation of the references to colour in this figure legend, the reader is referred to the web version of this article.)

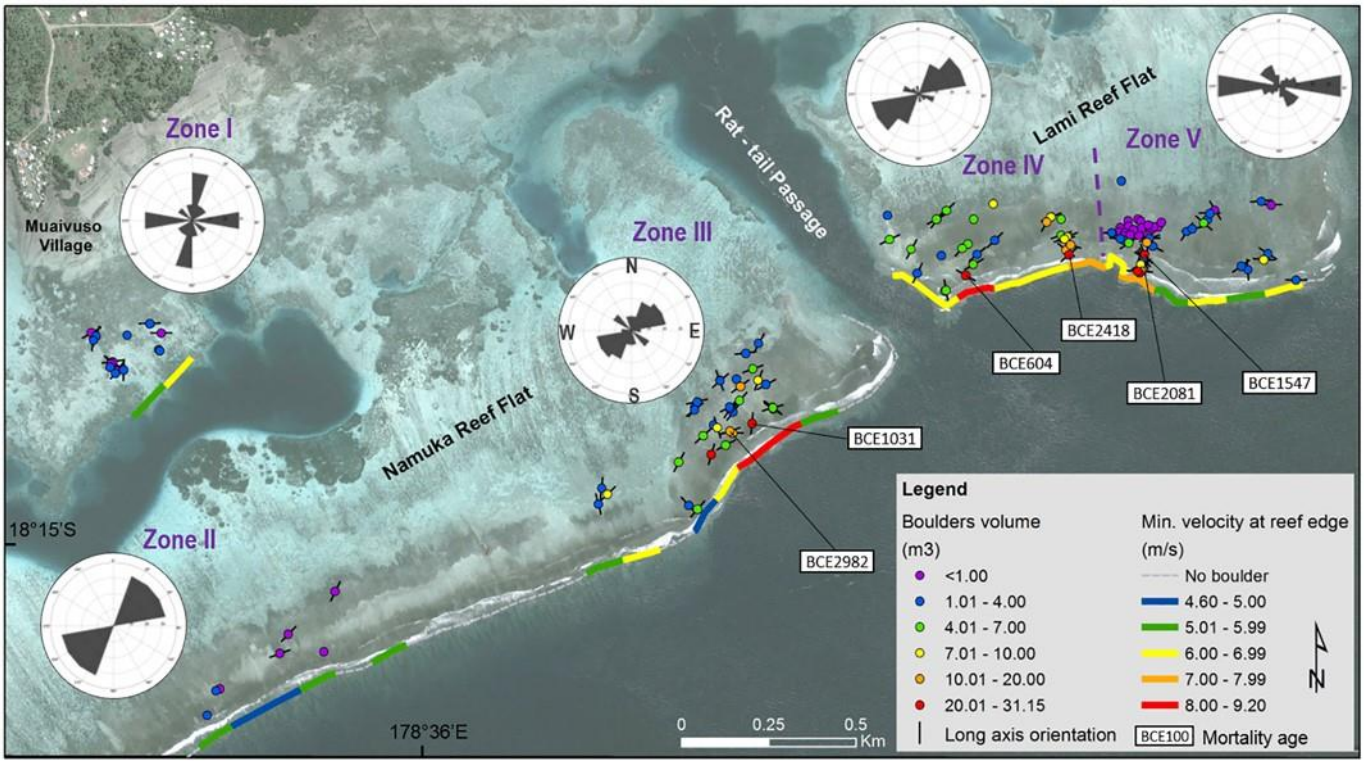

Fig. 5. Map of the study area showing analyses results. Rose diagrams of major orientation in each boulder field zone I to V are plotted with 180-degree rotational symmetry, with boulder orientations grouped into 20° grid bins. The minimum flow velocities (MFVs) required at the reef edge to lift clasts from the reef-edge framework (i.e., the presumed source) onto the reef flat are indicated by colour lines (see legend). Locations of six U-Th dated large boulders are marked by labels showing dating results (i.e., the coral mortality age). All samples were dated to BCE years. (For interpretation of the references to colour in this figure legend, the reader is referred to the web version of this article.)

for analysing reef-edge position over time. In the 1978 image, taken at the lowest altitude among all photos examined, 17 boulders are clearly visible, while nine and 17 boulders can be identified in the 1986 and 1994 photos, respectively (Table 3). Despite the improved satellite image quality, not all boulders measured in the field are visible on modern images because of insufficient resolution and high tide levels at the time of image acquisition. For example, boulders smaller than 1 m^3 are not discernible in a July 2016 satellite image.

Out of the 17 boulders visible on the 1978 photo, 11 were remobilised before 2005. Among those, seven moved distances of 12–65 m landward, while another four originally present on Lami Reef disappeared altogether. These clasts could have been broken into smaller pieces, or been washed into the 30 m deep Rat-tail Passage. A comparison of 1978 and 1986 aerial photos shows that all nine boulders visible were already present in 1978, hence there is no evidence for boulder reworking between 1978 and 1986. Similarly, although only a small number of boulders are visible on the 1994 aerial photo, their positions correspond with those in the post-2005 satellite images and field measurements in 2013. It can therefore be inferred that remobilising high-energy wave event(s) occurred sometime between 1986 and 1994.

The a-axis alignments of remobilised boulders are perpendicular or oblique to the direction of their most recent transport vectors (Table 3). These boulders' volumes range from 2.0 to 31.2 m^3 and all are shorter than 1.32 m in the vertical axis. Four boulders on Namuka Reef, including the third largest measured boulder (27.8 m^3), were moved NW for distances up to 66 m (Fig. 6). On Lami Reef, only three smaller boulders ƀ5.1 m^3 were remobilised, over shorter distances of 12–18 m towards the NE. The MFV estimations also suggest the flow velocity was higher on Namuka Reef than on Lami Reef (Fig. 6). The four boulders that disappeared before 2005 had unknown dimensions. To estimate the MFVs responsible for their removal, boulder heights were conservatively assumed to be 0.55 m, corresponding to the minimum c-axis measured for other nearby boulders at the site. The MFV required for their removal by sliding was at least 1.37–2.38 m s^{-1}.

Historical images were additionally valuable for revealing two changes in plan morphology of the Lami Reef front between 1954 and 1978 (Fig. 6). First, a reef scarp section approximately 1400 m^2 in area, with a maximum width of 22 m, disappeared. Second, an indentation in the reef outline located approximately 30 m E of the missing reef scarp retreated landward by 24 m, with the widening of an extended erosional groove occurring at the landward edge of the indentation. Since 1978, the outline of these two reef sections has remained unchanged.

4.4. Flow velocity estimations

The calculated minimum flow velocity (MFV) of each boulder represents the MFV experienced at the boulder source, i.e., the reef or lagoon edge. For illustration and analyses, the edges are divided into 100 m sections on the map in Fig. 5. The MFV required to initiate boulder transport from the submarine reef and emplace them onto the reef flats ranged from 2.80 to 9.29 m s^{-1} (Fig. 7a). Boulders in zones I and II are smaller, hence a velocity of 6 m s^{-1} was probably sufficient to emplace all boulders into these zones. In contrast, over half of all boulders in zones III to V (area closest to the submarine landslide scar) required at least 6 m s^{-1} to emplace them. Once deposited on the reef flat, boulders may be remobilised by all three transport modes, including sliding and rolling that require lower flow velocity to initiate movement. Wavegenerated MFVs between 0.89 and 2.38 m s^{-1} were likely necessary for sliding; 1.28–4.67 m s^{-1} for rolling (Fig. 7b).

Please cite this article as: Lau, A.Y.A., et al., Boulder emplacement and remobilisation by cyclone and submarine landslide tsunami waves near Suva City, Fiji, Sedimentary Geology (2017), https://doi.org/10.1016/j.sedgeo.2017.12.017

Table 3

Transport history of all boulders visible on 1978, 1986 and/or 1994 aerial photographs, identified by matching measured boulders in the field to the estimated boulder size and aerial view shapes in older aerial photos and post-2005 satellite images.

Boulder ID[a]	A-axis (m)	B-axis (m)	C-axis (m)	Volume (m^3)	Date of aerial/satellite image					Boulder transport history after 1978	Boulder orientation relative to transport direction[b]
					20 Jun. 1978	20 Jul. 1986	03 Oct. 1994	22 Jan. 2005	08 Jul. 2016		
NR142	3.74	2.61	1.30	8.8	v			N	v	Moved 65 m NW	Perpendicular
NR155	2.71	1.45	0.90	2.5	v			N	v	Moved 65 m NW	Sub-perpendicular
NR147	6.37	4.81	1.30	27.8	v	v	N	v	v	Moved 33 m NW	Sub-perpendicular
NR149	5.39	3.81	0.68	14.0	v	v	N	v	v	Moved 66 m NW	Sub-perpendicular
NR150	5.01	3.03	2.39	18.0			v	v	v	No movement	N/A
NR151	4.10	2.31	1.44	9.5			v	v	v	No movement	N/A
NR158	4.09	3.27	2.55	23.8			v	v	v	No movement	N/A
NR164	3.35	2.46	1.67	9.6			v	v	v	No movement	N/A
NR165	4.12	1.67	1.38	4.8			v	v	v	No movement	N/A
NR166	5.47	2.90	1.62	12.8			v	v	v	No movement	N/A
LR182	7.00	3.74	2.38	31.2			v	v	v	No movement	N/A
LR183	2.69	2.05	1.32	5.1	v		N	v	v	Moved 12 m NE	Oblique
LR192	2.96	2.62	1.64	6.4	v			v	v	No movement	N/A
LR193	3.11	2.80	1.45	8.8	v	v		v	v	No movement	N/A
A[c]	3.5	2				v					Disappeared
LR229	4.76	3.74	0.81	10.1	v	v		v	v	No movement	N/A
LR233	5.00	3.71	1.38	17.9			v	v	v	No movement	N/A
LR234	3.71	2.28	1.32	7.8			v	v	v	No movement	N/A
LR225 + LR226	2.30/2.84	1.39/1.77	0.90/1.11	2.0/3.9	v	v		N	v	Moved 12 m NE[d]	Sub-perpendicular
LR222	2.90	2.24	1.02	4.6	v			N	v	Moved 18 m NE	Oblique
B[c]	3	3				v					Disappeared
C[c]	2	1.5				v					Disappeared
D[c]	4	3				v					Disappeared
LR217	7.17	4.13	1.35	28.0	v	v		v	v	No movement	N/A
LR209	4.46	4.22	1.80	23.7	v			v	v	No movement	N/A
LR218	4.18	2.43	1.74	12.4	v			v	v	No movement	N/A

v = Visible on historical image. Visibility varies due to photo quality (resolution), altitude of camera, and tide level. Empty cell therefore means the boulder was not visible on the photo in question, but does not imply it was absent on the reefs. N = New boulder location after reworking.

[a] NR: Namuka Reef, LR: Lami Reef.

[b] Categorisation similar to Table 1. Boulder orientation ±10° to 90° (80–100°) to transport direction is considered 'perpendicular', ±30° is 'sub-perpendicular', around ±45° is oblique.

[c] Boulders not found in 2013. The a-b plane areas were estimated from 1978 aerial photo.

[d] The boulder seen on 1978 image may have broken into two boulders in the time period: it is uncertain whether it was a single boulder or two boulders arranged side by side in the 1978 photo as the image was not clear enough.

5. Discussion

5.1. Different mechanisms for boulder emplacement on NL Reefs

The clustering of large boulders around Rat-tail Passage in zones III–V (Fig. 3) supports the notion that these boulders were dislodged and deposited by the 1953 Suva tsunami (Houtz, 1962; Rahiman, 2006). Thus, the flow velocities calculated based on the large boulders in zones III-V can be used to reveal the magnitude and characteristics of the 1953 tsunami as the waves

Please cite this article as: Lau, A.Y.A., et al., Boulder emplacement and remobilisation by cyclone and submarine landslide tsunami waves near Suva City, Fiji, Sedimentary Geology (2017), https://doi.org/10.1016/j.sedgeo.2017.12.017

broke against the NL reefs. The tsunami flow velocity was the highest near the Rat-tail Passage opening, with flow exceeding 9 m s^{-1} impacting the SE-facing reef edges of zones III and IV. In zone V, wave-generated flow similarly attained velocities N5–8 m s^{-1}. The major orientations of large tsunami boulders measured in zones III and IV are similarly aligned ENE–WSW, indicating the strongest wave propagated from the SE. This wave propagation direction concurs with what would be expected if a landslide occurring at the Suva Canyon generated a tsunami, as was the case in 1953.

No boulders are located N250 m from the reef edge in these zones. In general, most wave energy (60–97%) is lost in shoaling, breaking, and reforming into bores at the reef edge (Gourlay, 1994; Parnell, 2011). Energy continues to diminish because of bottom friction across the reef flat (Massel and Gourlay, 2000; Péquignet et al., 2011). When a wave progressively dissipates across a reef flat, larger boulders are typically deposited first, while smaller boulders are deposited farther landward. The landward fining trend and short transport distances of boulders in zones III to V indicate that tsunami energy dissipated to a level that was insufficient to transport boulders farther inland. Such a rapid dissipation, however, does not explain the presence of boulders in zones I and II, which are located farthest from the tsunami source. Hence storm waves could be the alternative boulder emplacement mechanism in these two zones.

Boulder distribution in zone I on Namuka Reef is unusual because of its location on the back-reef behind Muaivuso Lagoon, approximately 1 km from the reef edge. Our results show that flat boulders tend to be deposited close to the boulder source. The clustering of flat clasts near the landward perimeter of Muaivuso Lagoon therefore is one key indicator that zone I boulders were sourced from the lagoon edge rather than from the distant seaward reef edge. Given the flat topography of Namuka Reef and the 2 m tidal range, high-energy waves impacting at high tide may be able to inundate areas far back on the reef flat (Gelfenbaum et al., 2011; Péquignet et al., 2011). As waves travel across the deep Muaivuso Lagoon into the shallower water beyond, they increase in speed and wave height (Lowe et al., 2009), allowing boulder delivery from the edge of the lagoon (Fig. 8).

Our simulation shows that when H_{so} N 7.8 m (as in a 1 in 50 year event), almost all boulders in zone II could potentially be lifted by storm waves from a joint-bounded setting; however, none could be lifted in zone I. Even if the offshore wave reaches 9.5 m in height, the simulated 3 m s^{-1} flow could only move one boulder by lifting from the lagoon to zone I. A more plausible explanation for zone I boulder emplacement is that boulders were originally coral heads and microatolls growing on the lagoon slope. Thus, a slower flow (b2 m s^{-1}) generated by a 1 in 30 year system like Cyclone Kina (H_{so} = 6.27), or a tsunami, could have transported the clasts by sliding or rolling into the back-reef area. The simulation also confirms Muaivuso villagers' descriptions of boulder remobilisations by post-1953 cyclones in both the back-reef area and close to the reef edge (Atkinson and Collen, 2000).

Please cite this article as: Lau, A.Y.A., et al., Boulder emplacement and remobilisation by cyclone and submarine landslide tsunami waves near Suva City, Fiji, Sedimentary Geology (2017), https://doi.org/10.1016/j.sedgeo.2017.12.017

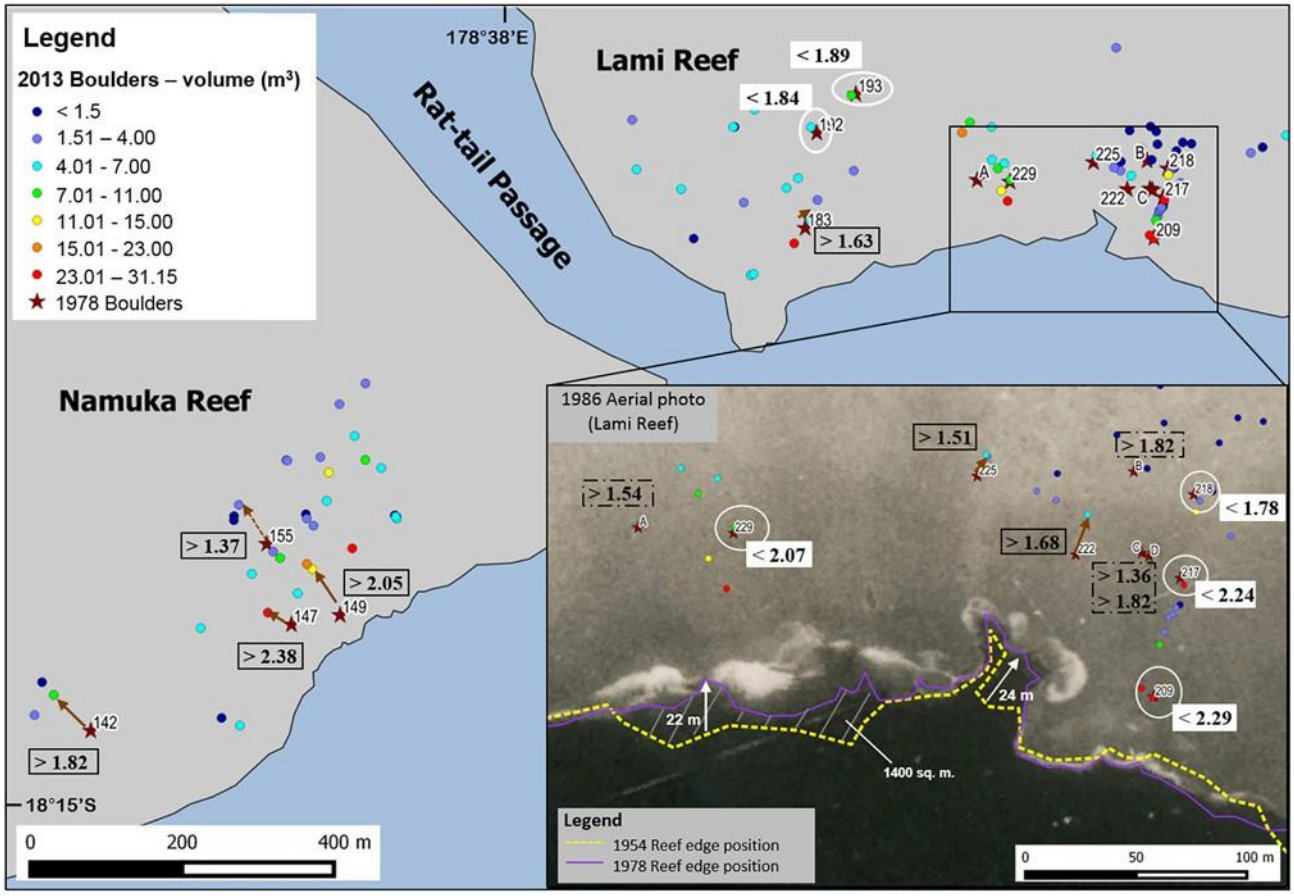

Fig. 6. Estimated flow velocities for a post-1953 high-energy wave (HEW) event that caused some boulder reworking after 1978. Boulders in white circles have remained in the same position since 1978. For stable boulders (over 1978–2013), the upper limits of flow velocities that would permit stability are given in white boxes. For remobilised boulders, brown arrows show movement vectors between 1978 and 2005, with a dashed arrow used where the transport path is less certain. The minimum flow velocity (MFV in m s^{-1}) to initiate boulder transport for each reworked boulder is written in a black box. The MFV value for sliding is used because remobilisation by sliding requires the lowest flow velocity. Dashed box outline indicates MFV based on estimated boulder dimensions for four older boulders (named A–D) that were transported away from the reef flat prior to fieldwork in 2013. The inset shows changes in the outline of the Lami Reef front between 1954 and 1978 aerial photos, plotted on the 1986 photo. Up to 24 m of reef scarp has been removed. The reef outline has remained stable since 1978. (For interpretation of the references to colour in this figure legend, the reader is referred to the web version of this article.)
Photos courtesy of Department of Lands and Surveys, Fiji.

The distribution of boulders on NL Reefs is similar to that in boulder fields on Ishigaki Island of Japan (Goto et al., 2010), as both sites comprise two boulder clusters — the first cluster consists of landward fining boulders deposited close to the reef edge; another group of boulders sits a few hundred metres farther landward. Moreover, groups of boulders at both sites are separated by deeper water bodies (2–4 m deep moats on Ishigaki Island; N20 m deep lagoon on NL Reefs), and the coasts are similarly prone to both storm and tsunami waves. Interestingly, in spite of these similarities, the distributions of tsunami boulders are distinctively different on Ishigaki Island and NL Reefs. On the coast of Ishigaki Island, it was determined that a tsunami, probably induced by a dip-slip fault plus a submarine landslide in 1771, was responsible for emplacing large boulders close to the shoreline (approximately 400–1300 m from reef edges). Long period tsunami waves are capable of long-distance clast transport, while short period storm waves account for the group of smaller boulders close to the reef edge (Goto et al., 2010; Miyazawa et al., 2012). In contrast, on NL Reefs, the 1953 tsunami could only transport boulders for short distances (b250 m) from the reef edge. This is probably a representation of the relatively short tsunami wavelength and wave period of events generated at this locality.

The short tsunami wavelength and period can be explained by the small source area and the small amount of material displaced in comparison to other tsunami sources. Firstly, tsunamis generated by submarine landslides are usually more dispersive with shorter periods and wavelengths due to smaller source areas, compared with those generated by earthquakes (Hammack, 1973; Watts et al., 2003). As the linear dimension of submarine landslides rarely exceeds 100 km, the wavelength of landslide tsunamis usually ranges from hundreds of m to tens of km; whereas lengths of earthquake tsunami waves can reach hundreds of km (Synolakis et al., 2002). Secondly, laboratory experiments have shown that wave periods increase with the size of the sliding body (Wiegel, 1955; Watts, 1998). The volume of the 1953 landslide mass was estimated at 60 million m^3, or 0.06 km^3, which can be considered small compared with other tsunamigenic landslides (Rahiman et al., 2007). For instance, the 1998 Papua New Guinea tsunami slump was estimated at 4 km^3 in volume and it generated a 44 s tsunami wave (Tappin et al., 2008). Although the tsunami wave period is also dependent on the landslide velocity and slope incline angle (Wiegel, 1955; Ward, 2001), it is logical to assume this small local landslide tsunami in 1953 was of relatively short wave period, likely at the scale of tens of s, hence resulting in clusters of tsunami boulders around the edges of the NL Reefs.

5.2. Post-1953 boulder remobilisation and reef-front landslide

The identification of boulder remobilisation on historical aerial photographs indicates the effect of probably one major high-wave energy

Please cite this article as: Lau, A.Y.A., et al., Boulder emplacement and remobilisation by cyclone and submarine landslide tsunami waves near Suva City, Fiji, Sedimentary Geology (2017), https://doi.org/10.1016/j.sedgeo.2017.12.017

(HEW) event in the study area between 1986 and 1994. According to the FMS cyclone reports, Cyclone Kina in January 1993 was the most

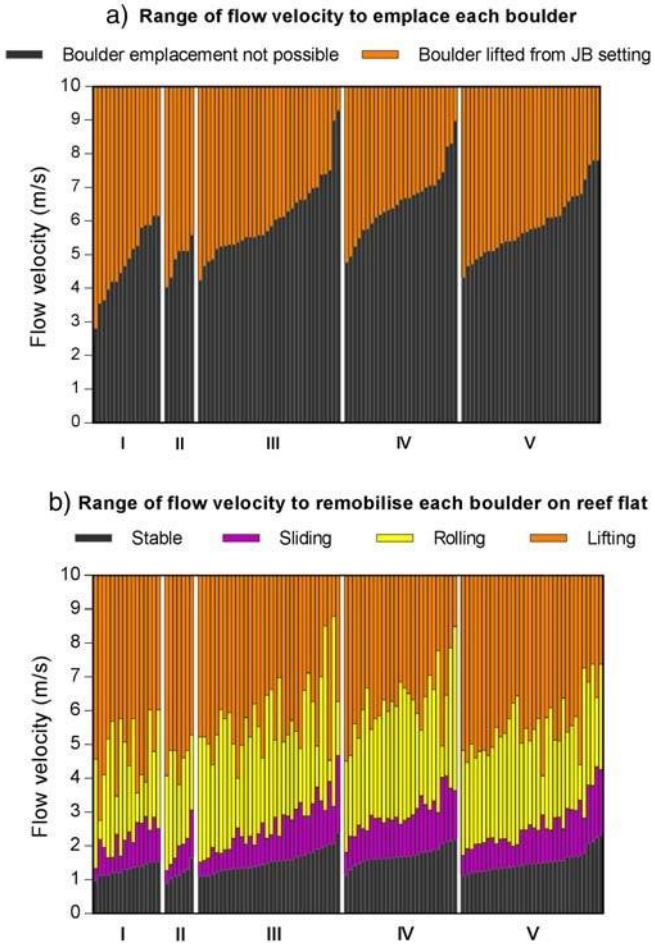

Fig. 7. Histogram of MFVs that are able to initiate boulder transport from (a) a jointbounded setting, and (b) on the unobstructed reef flat, sorted according to the designated five boulder field zones I to V on NL Reefs. Each vertical column represents an individual boulder. The MFV required for each transport mode is the value at the base of each colour bar (Nandasena et al., 2011). Data are arranged in order of increasing MFV required for transport by sliding. Boulders remain stable for flow velocities falling within the grey bars. (For interpretation of the references to color in this figure legend, the reader is referred to the web version of this article.)

severe storm for the SE coast of Viti Levu within this time frame (McGree et al., 2010). It was also the largest wave event in Suva from 1979 to 2015 (Bosserelle et al., 2015). Cyclone Kina waves are therefore the most likely responsible for boulder remobilisation. This category-4 tropical cyclone that tracked between Viti Levu and Vanua Levu Islands from NW to SE resulted in widespread coastal flooding in low-lying areas across Fiji (Prasad, 1993; FMS, 1996). While heavy rainfall, watershed flooding and record-breaking discharge in the Rewa River caused by Cyclone Kina were described in detail (McGree et al., 2010), the effects and characteristics of the associated cyclonic waves have not been reported. Our analyses of boulder remobilisation revealed that flow velocity on the studied reefs was N2 m s^{-1}, which was powerful enough to move a 28 m^3 boulder for 33 m. A 1D wave simulation also shows this event could have generated a 3.8 m s^{-1}flow at zone II reef edge (Fig. 8). In comparison, although the recent Cyclone Winston of February 2016 was a stronger category-5 system, its track direction towards northern Viti Levu spared Suva from the full brunt of enormous waves that devastated other places in the Fijian Islands (Terry and Lau, 2018). In villages behind our study site, several houses and trees were destroyed by strong wind. The villages were not flooded and no reef boulders were remobilised (A. Balawa of Waiqanaki Village, 6 June 2016, Personal Communication).

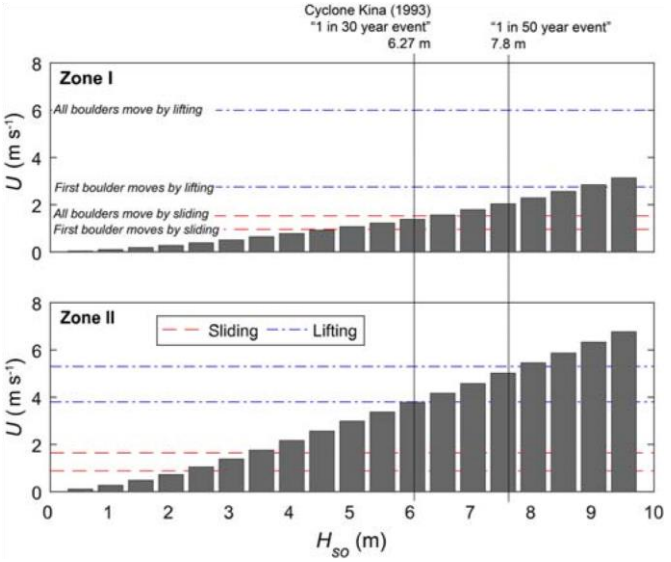

Fig. 8. Modelled storm wave flow velocity on NL Reefs along A-A′ transect. The maximum Eularian current velocity (u (m s^{-1})) was determined in zones I and II for each of the model runs from H_{so} (offshore significant wave height) = 0.5 m to 9.5 m, at 0.5 m interval. Dashed lines for sliding (the transport mode that requires lowest flow velocity) and lifting (the only transport mode for emplacing joint-bounded boulders) correspond to the lower and upper boundaries required to move boulders by the respective transport mode as presented in Fig. 7.

Not every remobilised boulder was orientated perpendicular to the flow direction, with some aligned oblique to the observed transport directions. This anomaly can be explained by the short-period of the wind-driven waves that moved them. Long axes of boulders may oscillate at the onset of transportation before eventually aligning perpendicular to flow, as demonstrated in wave tank experiments by Nandasena and Tanaka (2013). Taking into account the short transport distances (12–18 m) of the oblique-orientated boulders, it is likely that sufficient wave energy was not exerted for a long enough (unquantifiable) period of time to realign the long axes of the boulders with the flow direction as expected.

The discussions above and local villagers' reports consistently confirm that NL Reefs are subject to strong waves generated from both cyclone and tsunami waves. Making the tsunami more unpredictable in this area is the fact that the NL reefs may fail without the trigger of a noticeable earthquake. We revealed that sections of Lami reef front have failed between 1954 and 1978, a period without a significant earthquake occurring within 400 km of the locality (NOAA Global significant earthquake database, 2016). This slope failure was possibly a delayed response to the 1953 earthquake-landslide event. Indeed, following the 1953 event, the Fiji Geological Survey observed cracks near the seaward edges of the reef flats on the NL Reefs (The Fiji Times and Herald, 1953b). These cracks are mostly parallel to the curvature of the reef edge, suggesting they were tension features that developed when buttressing support of the reef front was removed at depth by the 1953 tsunamigenic submarine slope failure (Atkinson and Collen, 2000; Rahiman, 2006). Later, sometime between 1954 and 1978, the 1400 m^2 reef scarp section at Lami Reef failed along these lines of weakness, perhaps triggered by strong swells or minor seismic tremors — this time without generating a tsunami. Nevertheless, reef front failures are potentially tsunamigenic. Thus, the occurrence of non-earthquakeinduced reef-front

Please cite this article as: Lau, A.Y.A., et al., Boulder emplacement and remobilisation by cyclone and submarine landslide tsunami waves near Suva City, Fiji, Sedimentary Geology (2017), https://doi.org/10.1016/j.sedgeo.2017.12.017

collapse (in addition to earthquake-induced failure) must nonetheless factor into a full appreciation of local tsunami risk, and more specifically, in identifying possible future local tsunami sources in the vicinity of Suva. This risk is especially relevant as tension cracks running parallel to the modern reef front are still visible on NL Reefs today (Fig. 9).

Fig. 9. One of the tension cracks observed on Lami Reef. These features appeared after the 1953 tsunami as buttressing support below the reef was lost in the submarine slope failure.

5.3. Challenge in determining the timings of pre-historical landslide-tsunami events from boulder age-dating

Age-dating of boulders derived from the living reef framework may disclose the timing of the pre-historical HEW events that produced them, based on the assumption that the events in question killed living corals by removing them from their natural accommodation space at the reef front (Yu et al., 2004). This assumption has been validated by prior workers when mortality ages of corals in the fabric of large boulders coincide with known historical HEW events (e.g., Araoka et al., 2010; Yu et al., 2012).

However, identifying past occurrences of landslide-tsunamis from boulder age-dating is challenging. A fundamental problem that can hinder the application of coral mortality ages for timing of HEW events is that the method does not work if a HEW event quarries older parts of dead reef framework rather than living corals. Carbonate samples taken from six large boulder surfaces on NL Reefs were dated to the mid- to late-Holocene (approximately 5000–2600 year BP), in contradiction with local accounts suggesting these large boulders were only observed on the reefs after the 1953 tsunami. One hypothesis is that the villagers' reports were erroneous and the large boulders have been sitting on the reefs for thousands of years. However, this notion can be rejected considering the boulder erosion rate and past sea level. First, weathering of carbonate boulders on this intertidal reef flat is high. The tidal range is up to 2 m, and in situ mechanical abrasion by sandarmoured wave action is effective each tidal cycle. Moreover, we observed significant bioerosion by grazers such as sea urchins and chitons (Fig. 10). On the reef crest of nearby Nukubuco Reef (see Fig. 1 for location), Appana and Vuki (2003) measured bioerosion by Echinometra sp. sea urchins at rates of 35–37 $\times 10^{-3}$ kg m^{-2} day^{-1}, which extrapolates to 12.8–13.5 kg m^{-2} $year^{-1}$. With this high rate of bioerosion, it is not likely that the dated large boulders were preserved for 2600– 5000 years. Second, maximum sea level between 4630 and 3480 year

Please cite this article as: Lau, A.Y.A., et al., Boulder emplacement and remobilisation by cyclone and submarine landslide tsunami waves near Suva City, Fiji, Sedimentary Geology (2017), https://doi.org/10.1016/j.sedgeo.2017.12.017

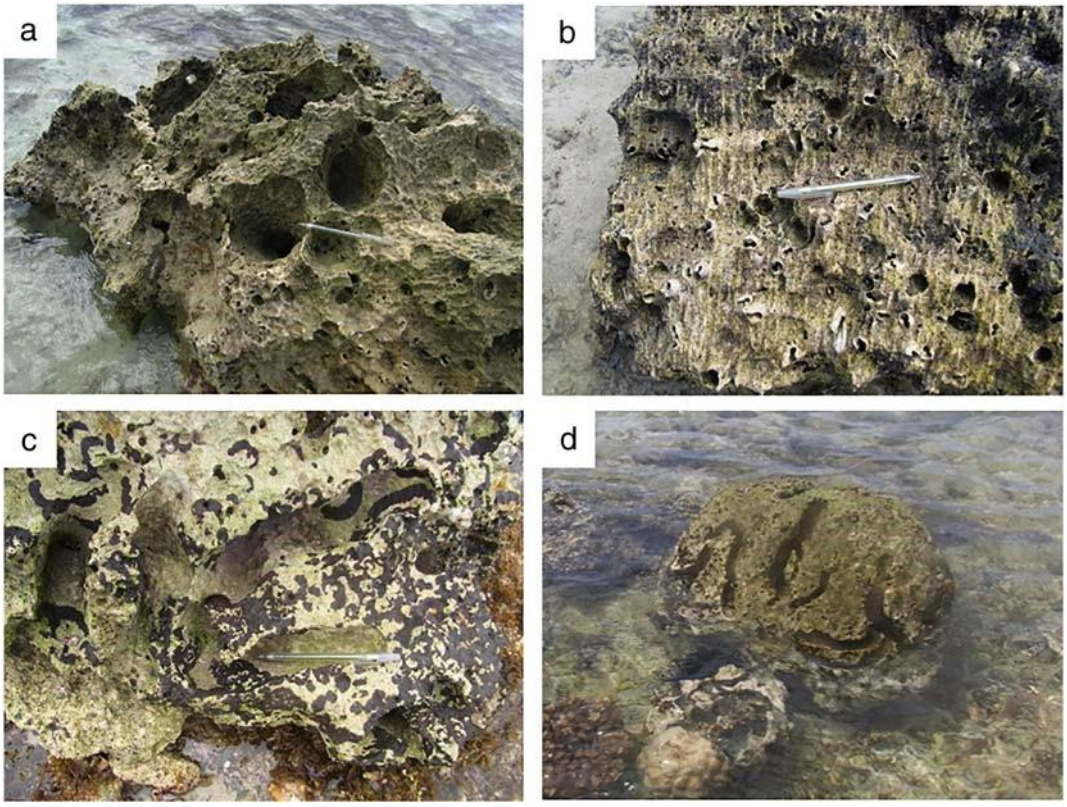

Fig. 10. Active bioerosion on carbonate boulders by various intertidal fauna: (a) chitons; (b) boreholes of Lithophaga mussels, with parallel traces possibly from chiton grazing; (c) and (d) deep sea-urchin crevices. Bioeroder identification following Kázmér and Taboroši (2012), kindly confirmed by Prof. Miklos Kázmér (November 2016, Personal Communication).

Please cite this article as: Lau, A.Y.A., et al., Boulder emplacement and remobilisation by cyclone and submarine landslide tsunami waves near Suva City, Fiji, Sedimentary Geology (2017), https://doi.org/10.1016/j.sedgeo.2017.12.017

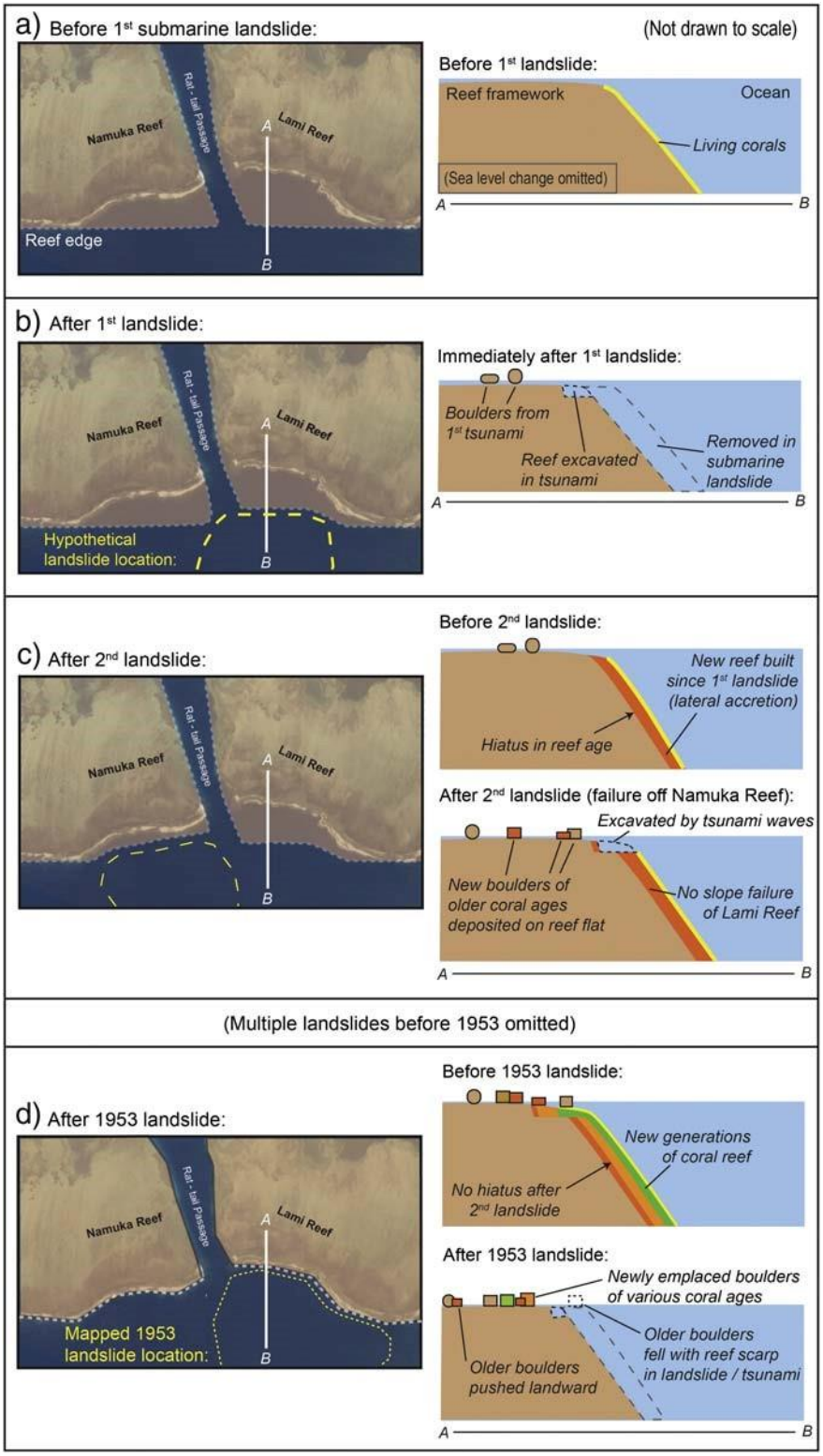

Fig. 11. Conceptual schema proposed to account simultaneously for the scalloped plan morphology of NL Reefs by tsunamigenic submarine landslides and the deposition of carbonate boulders of various ages on the reef flat by the associated tsunami. Left: plan views showing the hypothetical sequence of submarine landslides leading to the modern reef-front outline. Right: cross-sections of the reef front at Lami Reef. The timings of all pre-1953 submarine landslide events are unknown, so mid-late Holocene sea-level changes are omitted. (a) Before the earliest submarine landslide, youngest living corals are growing on the outermost reef front. (b) Landslide off Lami Reef removes the youngest section of reef. Tsunami generated by the landslide excavates the reef front and deposits carbonate boulders on the reef flats. Older, dead reef is now exposed at the reef front. Reef building by lateral accretion recommences, giving a hiatus in reef age. (c) Subsequent landslide fails off Namuka Reef, and the resulting tsunami quarries new boulders from Lami Reef front. Lateral reef building continues without a hiatus in reef age. (d) The 1953 tsunamigenic landslide fails offshore of Lami Reef following an earthquake. Some 30–50 m of Lami Reef front is removed in the landslide, taking with it some old boulders. Reef materials up to 5000 years old are simultaneously dislodged to form another set of new boulders.

Please cite this article as: Lau, A.Y.A., et al., Boulder emplacement and remobilisation by cyclone and submarine landslide tsunami waves near Suva City, Fiji, Sedimentary Geology (2017), https://doi.org/10.1016/j.sedgeo.2017.12.017

BP was 2.1 m above present sea level at SE Viti Levu (Lal and Nunn, 2011). If boulders were deposited on the reef flats at times of higher sea level, they would have been emplaced on a higher reef flat surface on which pedestals form beneath the boulders through thousands of years. The absence of any pedestals (rochers champignons), or traces of them, in turn support the theory that boulders were deposited in more recent times, which is in line with the observations reported.

Some potential sources of error in using carbonate age-dating for timing pre-historical HEW events have been discussed in the literature. For example, Yu et al. (2012) found that coral ages on the same boulder can differ by 30 years when different species of corals (one species with low uranium concentrations) are sampled for U-Th dating. Terry and Etienne (2014) demonstrated that ages of coral on the top and base of the same boulder may differ by a few hundred years. However in this study, the time discrepancy between dated coral mortality (i.e., 2982–604 BCE) and the actual event that emplaced the boulders (1953 CE) is on millennial timescales. This discrepancy raises two linked questions: (1) why boulder ages predate the 1953 tsunami by several millennia? and (2) might such knowledge be helpful in highlighting the scenarios of landslide-related reef-front retreat and associated tsunamigenic boulder deposition on coastal platforms in the study area?

To address such questions, we propose the conceptual model illustrated in Fig. 11. The bathymetry of Suva Canyon offshore from Rat-tail Passage, and the indented reef fronts around the passage opening, suggest the occurrence of several submarine slope failures at unknown times in the past, prior to the 1953 event (Rahiman, 2006). Scalloping and arcuate bight-like structures along reef margins are features of offshore collapse (Fairbridge, 1950; Mullins and Hine, 1989; Terry and Goff, 2013). Such collapses remove the youngest reef and expose older parts of the reef framework. Any tsunami generated by subsequent slope failure that occurs before significant lateral reef accretion by new growth in the landslide scar may then detach clasts from the older reef-front framework, as well as from adjoining younger segments of reef front. All clasts deposited on the reef flats will appear to be 'new' boulders. The model demonstrates how the mixed mortality ages of many coral boulders would be unrepresentative of the timing of the tsunami responsible for their production. In the current situation, different timing and locations of individual slope failures within the mapped composite landslide scar can thus explain how 1953 boulders exhibit a range of coral mortality ages and co-exist in relative proximity along the modern edge of NL Reefs. Given these limitations, the return period of tsunamis in the Suva remains uncertain. Our model has a major implication for similar studies of this nature. Attempting to ascertain the timing of past tsunami events by age-dating carbonate boulders derived from reef-front sources is ill-advised at sites where local submarine landslides are the cause of both reef-front collapse and tsunamigenesis. In such circumstances, the time difference between surface coral age and actual boulder transport can be on the order of a thousand years, hence alternative methods for identifying tsunami timings are needed.

6. Implications and conclusions

A boulder field created primarily by a landslide tsunami was investigated in detail for the first time. A main finding is that when a tsunami is triggered by a local reef failure, the boulder distribution is similar to that created by storm waves: it is characterised by short transport distance and clast landward-fining trends due to the relatively short tsunami wavelengths and periods. In the case of NL Reefs, tsunami boulders are distinguishable from storm boulders by their larger sizes because of the lower storm wave regime at this locality. However, this size difference is not always the same. The differentiation between storm and tsunami boulders would be challenging in places where storm waves are capable of emplacing larger boulders (e.g., blocks up to 71.5 m^3 were lifted by Typhoon Haiyan waves in the Philippines (Kennedy et al., 2017); a 60 m^3 boulder was emplaced by Cyclone Winston on Taveuni of Fiji (Terry and Lau, 2018) — both larger than the largest tsunami boulder identified in this study). Therefore, when investigating pre-historical HEW event characteristics from boulder deposits, it is easy to regard landslide tsunami boulders as storm boulders due to the higher occurrences of the latter event. As a result, the hazard of landslide tsunamis may be overlooked on some coastlines. Indeed, many local tsunamis may not be recorded if the coastline is sparsely populated. A tsunami at Mangaia in the Cook Islands in 2010, probably caused by a submarine landslide, is a modern example (Goff, 2011). The author highlighted that volcanic-associated submarine slope failures are relatively common among Pacific island countries due to the volcanic origin of many oceanic islands. Such failures are potentially tsunamigenic, but may only be identified by a detailed bathymetric survey for submarine landslide scars, and with the presence of boulder and fine sediment deposits onshore. This current study of the NL Reefs landslide tsunami deposits can be used as a reference set in identifying possible pre-historical local submarine landslide tsunami occurrences. This reference set will be particularly useful for regions where storms and earthquakes are rare, such as the equatorial central Pacific.

An unexpected finding is that age-dating of the largest tsunami boulders yields coral mortality ages that are inconsistent with the 1953 event that was responsible for their emplacement. To explain this, we propose a conceptual model (Fig. 11) based on repeated episodes of tsunamigenic submarine landslides, which remove sections of the reef front through collapse. The model accounts for the discrepancies of millennial proportions between tsunami timing and the 5000–2600 BP ages of the coral fabric comprising the 'new' clasts that were deposited. Our principal recommendation is that where local tsunamigenic submarine failures are the cause of the reef-front collapse, as demonstrated by the resulting arcuate scarps in the reef plan geomorphology, age-dating of the reef-derived clastic deposits should not be used as a proxy for determining the timing of either the landslides or the tsunamis.

Although the recurrence interval of tsunamis is still undetermined, Suva city and its surrounding coastlines are still at risk of tsunamis generated by landslides along the steep headward margins of the submarine Suva Canyon that lies immediately offshore. Tsunamigenic submarine slope failures may occur with, and possibly without, accompanying earthquakes. Waves from tropical cyclones also play a role in reef front erosion. Future work should focus on identifying the return period of the Suva tsunamis, and should include the threat of nonearthquake-induced slope failures in coastal risk assessments and preparedness initiatives in the SE Viti Levu area as coastal development rapidly expands.

Supplementary data to this article can be found online at https://doi.org/10.1016/j.sedgeo.2017.12.017.

Acknowledgements

We thank Dave Tappin and another anonymous reviewer, as well as the Managing guest-editor of this issue, for their constructive comments that greatly improved this manuscript. Jeremaia Buinimasi of the Department of Lands and Surveys, Fiji, is thanked for his technical assistance with aerial photographs. Mitieli Naucabalavu gave kind assistance with field measurements. Appreciation is extended to the chiefs and villagers of Muaivuso and Waiqanaki for help, hospitality and permission to work on their local coastlines. Chris Roelfsema is thanked for sharing useful data on reef geomorphic zones. AYA Lau was supported by the National University of Singapore Research Scholarship and the Hui Yin Hing Fellowship 2011-2015 for her PhD study that comprised this project. JP Terry duly acknowledges financial support from Zayed University for fieldwork expeditions (RIF grant no. R17036).

Please cite this article as: Lau, A.Y.A., et al., Boulder emplacement and remobilisation by cyclone and submarine landslide tsunami waves near Suva City, Fiji, Sedimentary Geology (2017), https://doi.org/10.1016/j.sedgeo.2017.12.017

References

Appana, S., Vuki, V.C., 2003. A novel method for assessing bioerosion by the sea urchin Echinometra sp. on a Fijian reef. The South Pacific Journal of Natural Science 21, 25–30.

Araoka, D., Inoue, M., Suzuki, A., Yokoyama, Y., Edwards, R.L., Cheng, H., Matsuzaki, H., Kan, H., Shikazono, N., Kawahata, H., 2010. Historic 1771 Meiwa tsunami confirmed by high-resolution U/Th dating of massive Porites coral boulders at Ishigaki Island in the Ryukyus, Japan. Geochemistry, Geophysics, Geosystems 11:1–11. https://doi.org/10.1029/2009GC002893.

Araoka, D., Yokoyama, Y., Suzuki, A., Goto, K., Miyagi, K., Miyazawa, K., Matsuzaki, H., Kawahata, H., 2013. Tsunami recurrence revealed by Porites coral boulders in the southern Ryukyu Islands, Japan. Geology 41, 919–922.

Atkinson, J.E., Collen, J.D., 2000. Environmental setting of Namuka Reef, Suva Fiji Islands. SOPAC Technical Report 324. SOPAC, Suva, Fiji, p. 20.

Baldock, T.E., Golshani, A., Callaghan, D.P., Saunders, M.I., Mumby, P.J., 2014. Impact of sealevel rise and coral mortality on the wave dynamics and wave forces on barrier reefs. Marine Pollution Bulletin 83, 155–164.

Blott, S.J., Pye, K., 2008. Particle shape: a review and new methods of characterization and classification. Sedimentology 55, 31–63.

BoM, CSIRO, 2014. Australian Bureau of Meteorology and CSIRO. Climate Variability, Extremes and Change in the Western Tropical Pacific: New Science and Updated Country Reports. Pacific-Australia Climate Change Science and Adaptation Planning Program Technical ReportAustralian Bureau of Meteorology and Commonwealth Scientific and Industrial Research Organisation, Melbourne, Australia.

BoM, 2015. Australian Government Bureau of Meteorology. Pacific Sea Level Monitoring Project Tide Calendars – Fiji Suva. http://www.bom.gov.au/oceanography/projects/spslcmp/tidecalendars.shtml, Accessed date: 15 July 2016.

Bosserelle, C., Reddy, S., Lal, D., 2015. WACOP Wave Climate Reports. Secretariat of the Pacific Community, Fiji, Suva http://gsd.spc.int/wacop/, Accessed date: 30 May 2017.

Buckley, M., Lowe, R., Hansen, J., 2014. Evaluation of nearshore wave models in steep reef environments. Ocean Dynamics 64, 847–862.

Cailleux, A., 1945. Distinction des galets marins et fluviatiles. Bulletin de la Societe Geologique de France 5, 375–404.

Carter, W.N., Chung, J.M., Gupta, S.P., 1991. South Pacific country study. http://cidbimena.desastres.hn/pdf/eng/doc4760/doc4760.htm, Accessed date: 1 February 2017.

Cheng, H., Edwards, R.L., Hoff, J., Gallup, C.D., Richards, D.A., Asmerom, Y., 2000. The halflives of uranium-234 and thorium-230. Chemical Geology 169, 17–33.

Clark, T.R., Roff, G., Zhao, J., Feng, Y., Done, T.J., Pandolfi, J.M., 2014a. Testing the precision and accuracy of the U–Th chronometer for dating coral mortality events in the last 100 years. Quaternary Geochronology 23, 35–45.

Clark, T.R., Zhao, J., Roff, G., Feng, Y., Done, T.J., Nothdurft, L.D., Pandolfi, J.M., 2014b. Discerning the timing and cause of historical mortality events in modern Porites from the Great Barrier Reef. Geochimica et Cosmochimica Acta 138, 57–80.

Collen, J.D., Atkinson, J.E., Patterson, J.E., 2011. Trace metal partitioning in a nearshore tropical environment: geochemistry of carbonate reef flats adjacent to Suva Harbor, Fiji Islands. Pacific Science 65, 95–107.

QGIS Development Team, 2013. QGIS Geographic Information System. Open Source Geospatial Foundation Project http://qgis.osgeo.org.

Dunham, R.J., 1962. Classification of carbonate rocks according to depositional texture. In: Ham, W.E. (Ed.), Classification of Carbonate Rocks. American Association of Petroleum Geologists Memoir, pp. 108–121.

Edwards, R.L., Chen, J.H., Wasserburg, G.J., 1987. ^{238}U–^{234}U–^{230}Th–^{232}Th systematics and the precise measurement of time over the past 500,000 years. Earth and Planetary Science Letters 81, 175–192.

Engel, M., May, S.M., 2012. Bonaire's boulder fields revisited: evidence for Holocene tsunami impact on the Leeward Antilles. Quaternary Science Reviews 54, 126–141.

Etienne, S., Terry, J.P., 2012. Coral boulders, gravel tongues and sand sheets: features of coastal accretion and sediment nourishment by Cyclone Tomas (March 2010) on Taveuni Island, Fiji. Geomorphology 175–176, 54–65.

Etienne, S., Buckley, M., Paris, R., Nandasena, A.K., Clark, K., Strotz, L., Chagué-Goff, C., Goff, J., Richmond, B., 2011. The use of boulders for characterising past tsunami: lessons from the 2004 Indian Ocean and 2009 South Pacific tsunami. Earth-Science Reviews 107, 76–90.

Fairbridge, R.W., 1950. Landslide patterns on oceanic volcanoes and atolls. The Geographical Journal 115, 84–88.

Fiji Meteorological Service (FMS), 1996. Tropical cyclones affecting Fiji May 1985 to April 1985. FMS Information Sheet 122.

FMS, 2001. List of floods occurring in the Fiji Islands between 1840 and 2000. FMS Information Sheet No. 125.

FMS, 2006. The climate of Fiji. http://www.met.gov.fj/ClimateofFiji.pdf, Accessed date: 14 September 2017.

Gelfenbaum, G., Apotsos, A., Stevens, A.W., Jaffe, B., 2011. Effects of fringing reefs on tsunami inundation: American Samoa. Earth-Science Reviews 107, 12–22.

Gienko, G.A., Terry, J.P., 2014. Three-dimensional modeling of coastal boulders using multi-view image measurements. Earth Surface Processes and Landforms 39, 853–864.

Goff, J., 2011. Evidence of a previously unrecorded local tsunami, 13 April 2010, Cook Islands: implications for Pacific Island countries. Natural Hazards and Earth System Sciences 11, 1371–1379.

Google Earth, 2005. Suva, Fiji. DigitalGlobe 2016. http://www.earth.google.com (January 22).

Goto, K., Chavanich, S.A., Imamura, F., Kunthasap, P., Matsui, T., Minoura, K., Sugawara, D., Yanagisawa, H., 2007. Distribution, origin and transport process of boulders deposited by the 2004 Indian Ocean tsunami at Pakarang Cape, Thailand. Sedimentary Geology 202, 821–837.

Goto, K., Miyagi, K., Kawamata, H., Imamura, F., 2010. Discrimination of boulders deposited by tsunami and storm waves at Ishigaki Island, Japan. Marine Geology 269, 34–45.

Goto, K., Miyagi, K., Kawana, T., Takahashi, J., Imamura, F., 2011. Emplacement and movement of boulders by known storm waves — field evidence from the Okinawa Islands, Japan. Marine Geology 283, 66–78.

Gourlay, M.R., 1994. Wave transformation on a coral reef. Coastal Engineering 23, 17–42.

Hall, A.M., Hansom, J.D., Williams, D.M., Jarvis, J., 2006. Distribution, geomorphology and lithofacies of cliff-top storm deposits: examples from the high-energy coasts of Scotland and Ireland. Marine Geology 232, 131–155.

Hamburger, M.W., Everingham, I.B., Isacks, B.L., Barazangi, M., 1990. Seismicity and crustal structure of the Fiji Platform, Southwest Pacific. Journal of Geophysical Research 95, 2553–2573.

Hammack, J.L., 1973. A note on tsunamis: their generation and propagation in an ocean of uniform depth. Journal of Fluid Mechanics 60, 769–799.

Houtz, R.E., 1962. 1953 Suva earthquake and tsunami. Bulletin of the Seismological Society of America 52, 1–12.

Imamura, F., Goto, K., Ohkubo, S., 2008. A numerical model for the transport of a boulder by tsunami. Journal of Geophysical Research 113:1–12. https://doi.org/10.1029/ 2007JC004170.

Kázmér, M., Taboroši, D., 2012. Bioerosion on the small scale – examples from the tropical and subtropical littoral. Hantkeniana 7, 37–94.

Kennedy, A.B., Mori, N., Yasuda, T., Shimozono, T., Tomiczek, T., Donahue, A., Shimura, T., Imai, Y., 2017. Extreme block and boulder transport along a cliffed coastline (Calicoan Island, Philippines) during Super Typhoon Haiyan. Marine Geology 383, 65–77.

Lal, K.K., Nunn, P.D., 2011. Holocene sea levels and coastal change, south-west Viti Levu Island, Fiji. Australian Geographer 42, 41–51.

Lau, A.Y.A., Terry, J.P., Ziegler, A.D., Switzer, A.D., Lee, Y., Etienne, S., 2016. Understanding the history of extreme wave events in the Tuamotu Archipelago of French Polynesia from large carbonate boulders on Makemo Atoll, with implications for future threats in the central South Pacific. Marine Geology 380, 174–190.

Liu, E., Zhao, J., Feng, Y., Leonard, N.D., Clark, T.R., Roff, G., 2016. U-Th age distribution of coral fragments from multiple rubble ridges within the Frankland Islands, Great Barrier Reef: implications for past storminess history. Quaternary Science Reviews 143, 51–68.

Lowe, R.J., Falter, J.L., Monismith, S.G., Atkinson, M.J., 2009. Wave-driven circulation of a coastal reef-lagoon system. Journal of Physical Oceanography 39, 873–893.

Massel, S.R., Gourlay, M.R., 2000. On the modelling of wave breaking and set-up on coral reefs. Coastal Engineering 39, 1–27.

May, S.M., Engel, M., Brill, D., Cuadra, C., Lagmay, A.M.F., Santiago, J., 2015. Block and boulder transport in Eastern Samar (Philippines) during Supertyphoon Haiyan. Earth Surface Dynamics Discussions 3, 739–771.

McGree, S., Yeo, S.W., Devi, S., 2010. Flooding in the Fiji Islands between 1840 and 2009. Risk Frontiers Report. Risk Frontiers, Australia (69 pp.).

Miyazawa, K., Goto, K., Imamura, F., 2012. Re-evaluation of the 1771 Meiwa Tsunami source model, Southern Ryukyu Islands, Japan. In: Yamada, Y., Kawamura, K., Ikehara, K., Ogawa, Y., Urgeles, R., Mosher, D., Chaytor, J., Strasser, M. (Eds.), Submarine Mass Movements and Their Consequences: 5th International Symposium. Springer Netherlands, Dordrecht, pp. 497–506.

Monismith, S.G., Herdman, L.M.M., Ahmerkamp, S., Hench, J.L., 2013. Wave transformation and wave-driven flow across a steep coral reef. Journal of Physical Oceanography 43, 1356–1379.

Mullins, H.T., Hine, A.C., 1989. Scalloped bank margins: beginning of the end for carbonate platforms? Geology 17, 30–33.

Nandasena, N.A.K., Tanaka, N., 2013. Boulder transport by high energy: numerical modelfitting experimental observations. Ocean Engineering 57, 163–179.

Nandasena, N.A.K., Paris, R., Tanaka, N., 2011. Reassessment of hydrodynamic equations: minimum flow velocity to initiate boulder transport by high energy events (storms, tsunami). Marine Geology 281, 70–84.

Nielsen, P., 1992. Coastal Bottom Boundary Layers and Sediment Transport. World Scientific, Singapore.

NOAA, 2016. Global significant earthquake database. https://www.ngdc.noaa.gov/nndc/struts/form?t=101650&s=1&d=1, Accessed date: 27 November 2016.

Please cite this article as: Lau, A.Y.A., et al., Boulder emplacement and remobilisation by cyclone and submarine landslide tsunami waves near Suva City, Fiji, Sedimentary Geology (2017), https://doi.org/10.1016/j.sedgeo.2017.12.017

NOAA historical tsunami database, 2016. Tsunami data and information. http://www.ngdc.noaa.gov/hazard/tsu.shtml, Accessed date: 27 November 2016.

Noormets, R., Crook, K.A.W., Felton, E.A., 2004. Sedimentology of rocky shorelines: 3. Hydrodynamics of megaclast emplacement and transport on a shore platform, Oahu, Hawaii. Sedimentary Geology 172, 41–65.

Nunn, P.D., Peltier, W.R., 2001. Far-field test of the ICE-4G model of global isostatic response to deglaciation using empirical and theoretical Holocene sea-level reconstructions for the Fiji Islands, Southwestern Pacific. Quaternary Research 55, 203–214.

Paris, R., Wassmer, P., Sartohadi, J., Lavigne, F., Barthomeuf, B., Desgages, E., Grancher, D., Baumert, P., Vautier, F., Brunstein, D., 2009. Tsunamis as geomorphic crises: lessons from the December 26, 2004 tsunami in Lhok Nga, West Banda Aceh (Sumatra, Indonesia). Geomorphology 104, 59–72.

Parnell, K.E., 2011. Fringing reef circulation. In: Hopley, D. (Ed.), Encyclopedia of Modern Coral Reefs. Encyclopedia of Earth Sciences Series. Springer Netherlands, Dordrecht, pp. 427–430.

Pearce, H., 2008. SOPAC/GA Tsunami Hazard & Risk Assessment Project Report 05 – Inventory of Geospatial Data and Options for Tsunami Inundation & Risk Modelling – Fiji Islands.

Péquignet, A.-C., Becker, J.M., Merrifield, M.A., Boc, S.J., 2011. The dissipation of wind wave energy across a fringing reef at Ipan, Guam. Coral Reefs 30, 71–82.

Phinn, S.R., Roelfsema, C.M., Mumby, P.J., 2012. Multi-scale, object-based image analysis for mapping geomorphic and ecological zones on coral reefs. International Journal of Remote Sensing 33, 3768–3797.

Prasad, R., 1993. Tropical Cyclone Kina Report. Fiji Meteorological Service http://www.pacificdisaster.net/pdnadmin/data/original/JB_DM393g_FJI_1993_TC_Kina.pdf, Accessed date: 20 June 2017.

Prasad, G., Rynn, J., Kaloumaira, A., 2000. Tsunami mitigation for the City of Suva, Fiji. Science of Tsunami Hazards 18, 35–54.

Rahiman, T.I.H., 2006. Neotectonics, Seismic and Tsunami Hazards, Viti Levu, Fiji. (Ph.D. Thesis). University of Canterbury, New Zealand.

Rahiman, T.I.H., Pettinga, J.R., 2006. The offshore morpho-structure and tsunami sources of the Viti Levu Seismic Zone, southeast Viti Levu, Fiji. Marine Geology 232, 203–225.

Rahiman, T.I.H., Pettinga, J.R., Watts, P., 2007. The source mechanism and numerical modelling of the 1953 Suva tsunami, Fiji. Marine Geology 237, 55–70.

Reed, A.W., Hames, I., 1967. Myths and Legends of Fiji and Rotuma. Reed, Wellington, Auckland.

Roelfsema, C., Phinn, S., 2008. Evaluating eight field and remote sensing approaches for mapping the benthos of three different coral reef environments in Fiji. In: Robert, J.F., Serge, A., Hiroshi, K., Mervyn, J.L., Delu, P., Trevor, P. (Eds.), Remote Sensing of Inland, Coastal, and Oceanic Waters. Proceeding of SPIE, Remote Sensing of Inland, Coastal, and Oceanic Waters, Noumea, New Caledonia 71500F1-71500F14.

Roelvink, D., Van Dongeren, A., McCall, R., Hoonhout, B., Van Rooijen, A., Van Geer, P., De Vet, L., Nederhoff, K., Quataert, E., 2015. Xbeach Technical Reference: Kingsday Release. Deltares, Technical report, Delft, The Netherlands.

Rogers, J.S., Monismith, S.G., Koweek, D.A., Dunbar, R.B., 2016. Wave dynamics of a Pacific Atoll with high frictional effects. Journal of Geophysical Research: Oceans 121, 350–367.

Salzmann, L., Green, A., 2012. Boulder emplacement on a tectonically stable, wavedominated coastline, Mission Rocks, northern KwaZulu-Natal, South Africa. Marine Geology 323-325, 95–106.

Scicchitano, G., Monaco, C., Tortorici, L., 2007. Large boulder deposits by tsunami waves along the Ionian coast of south-eastern Sicily (Italy). Marine Geology 238, 75–91.

Scicchitano, G., Pignatelli, C., Spampinato, C.R., Piscitelli, A., Milella, M., Monaco, C., Mastronuzzi, G., 2012. Terrestrial laser scanner techniques in the assessment of tsunami impact on the Maddalena peninsula (south-eastern Sicily, Italy). Earth, Planets and Space 64, 889–903.

Shah-Hosseini, M., Saleem, A., Mahmoud, A.M.A., Morhange, C., 2016. Coastal boulder deposits attesting to large wave impacts on the Mediterranean coast of Egypt. Natural Hazards 83, 849–865.

Singh, A., Aung, T., 2008. Salinity, temperature and turbidity structure in the Suva lagoon, Fiji. American Journal of Environmental Sciences 4, 266–275.

Smart, P.L., 1991. Uranium series dating. In: Smart, P.L., Frances, P.D. (Eds.), Quaternary Dating Methods – A User's Guide. Technical Guide 4. Quaternary Research Association, Cambridge, pp. 45–83.

Song, Y.T., Chen, J., Fu, L.-L., Zlotnicki, V., Shum, C.K., Yi, Y., Hjorleifsdottir, V., 2005. The 26 December 2004 tsunami source estimated from satellite radar altimetry and seismic waves. Geophysical Research Letters 32:1–5. https://doi.org/10.1029/2005GL023683.

Soria, J.L.A., Switzer, A.D., Pilarczyk, J.E., Tang, H., Weiss, R., Siringan, F., Manglicmot, M., Gallentes, A., Lau, A.Y.A., Lin, A.C.Y., Ling, T.K.W., 2017. Surf beat during Typhoon Haiyan deposits two distinct sediment assemblages on the carbonate coast of Hernani, Samar, central Philippines. Marine Geology http://www.sciencedirect.com/science/article/pii/S0025322717304036 (in press).

South Pacific Disaster Reduction Programme (SPDRP), 2002. Suva Earthquake Risk Management Scenario Pilot Project (SERMP) – Part I Summary Report (58 pp.).

Southern Hemisphere Tropical Cyclone Data Portal, 2011. Pacific Climate Change Science Program. Bureau of Meteorology, Melbourne, Australia http://www.bom.gov.au/cyclone/history/tracks/, Accessed date: 23 February 2016.

Spiske, M., Bahlburg, H., 2011. A quasi-experimental setting of coarse clast transport by the 2010 Chile tsunami (Bucalemu, Central Chile). Marine Geology 289, 72–85.

Synolakis, C.E., Bardet, J.-P., Borrero, J.C., Davies, H.L., Okal, E.A., Silver, E.A., Sweet, S., Tappin, D.R., 2002. The slump origin of the 1998 Papua New Guinea Tsunami. Proceedings of the Royal Society of London, Series A: Mathematical, Physical and Engineering Sciences 458, 763–789.

Tappin, D.R., Watts, P., Grilli, S.T., 2008. The Papua New Guinea tsunami of 17 July 1998: anatomy of a catastrophic event. Natural Hazards and Earth System Sciences 8, 243–266.

Terry, J.P., 2007. Tropical Cyclones: Climatology and Impacts in the South Pacific. Springer, New York (210 pp.).

Terry, J.P., Etienne, S., 2014. Potential for timing high-energy marine inundation events in the recent geological past through age-dating of reef boulders in Fiji. Geoscience Letters 1:14. https://doi.org/10.1186/s40562-014-0014-8.

Terry, J.P., Gienko, G., 2010. Climatological aspects of South Pacific tropical cyclones, based on analysis of the RSMC-Nadi (Fiji) regional archive. Climate Research 42, 223–233.

Terry, J.P., Goff, J., 2013. One hundred and thirty years since Darwin: reshaping the theory of atoll formation. The Holocene 23, 613–617.

Terry, J.P., Lau, A.Y.A., 2018. Magnitudes of nearshore waves generated by tropical cyclone Winston, the strongest landfalling cyclone in South Pacific records. Unprecedented or unremarkable? Sedimentary Geology http://www.sciencedirect.com/science/article/pii/S0037073817302282 (in press).

Terry, J.P., Dunne, K., Jankaew, K., 2016. Prehistorical frequency of high-energy marine inundation events driven by typhoons in the Bay of Bangkok (Thailand), interpreted from coastal carbonate boulders. Earth Surface Processes and Landforms 41, 553–562.

The Fiji Times & Herald, 1953a. Felt Quake While at Sea in Cutter – Mr G.Houng Lee's Experience, September 24.

The Fiji Times & Herald, 1953b. Experts Review Causes and Effect of 1953 Earthquake, October 7.

Thomas, C., Burbidge, D., Cummins, P., 2007. A preliminary study into the Tsunami Hazard faced by Southwest Pacific Nations. Report by Risk and Impact Analysis Group. Geoscience Australia, Australian Government (38 pp.).

Walker, M., 2005. Quaternary Dating Methods. John Wiley & Sons Ltd., Chichester.

Ward, S.N., 2001. Landslide tsunami. Journal of Geophysical Research: Solid Earth (1978–2012) 106, 11201–11215.

Watt, S., Jaffe, B., Morton, R., Richmond, B., Gelfenbaum, G., 2010. Description of extremewave deposits on the northern coast of Bonaire, Netherlands Antilles. U.S. Geological Survey Open-File Report 2010-1180. U.S. Geological Survey, Unites States (64 pp.).

Watts, P., 1998. Wavemaker curves for tsunamis generated by underwater landslides. Journal of Waterway, Port, Coastal, and Ocean Engineering 124, 127–137.

Watts, P., Grilli, S.T., Kirby, J.T., Fryer, G.J., Tappin, D.R., 2003. Landslide tsunami case studies using a Boussinesq model and a fully nonlinear tsunami generation model. Natural Hazards and Earth System Sciences 3, 391–402.

Wentworth, C.K., 1922. A scale of grade and class terms for clastic sediments. Journal of Geology 30, 377–392.

Wiegel, R.L., 1955. Laboratory studies of gravity waves generated by the movement of a submerged body. Eos, Transactions of the American Geophysical Union 36, 759–774.

Yamada, M., Fujino, S., Goto, K., 2014. Deposition of sediments of diverse sizes by the 2011 Tohoku-oki tsunami at Miyako City, Japan. Marine Geology 358, 67–78.

Yu, K.-F., Zhao, J.-X., Collerson, K.D., Shi, Q., Chen, T.-G., Wang, P.-X., Liu, T.-S., 2004. Storm cycles in the last millennium recorded in Yongshu Reef, southern South China Sea. Palaeogeography, Palaeoclimatology, Palaeoecology 210, 89–100.

Yu, K., Zhao, J., Shi, Q., Meng, Q., 2009. Reconstruction of storm/tsunami records over the last 4000 years using transported coral blocks and lagoon sediments in the southern South China Sea. Quaternary International 195, 128–137.

Yu, K., Zhao, J., Roff, G., Lybolt, M., Feng, Y., Clark, T., Li, S., 2012. High-precision U-series ages of transported coral blocks on Heron Reef (southern Great Barrier Reef) and storm activity during the past century. Palaeogeography, Palaeoclimatology, Palaeoecology 337-338, 23–36.

Zhao, J., Neil, D.T., Feng, Y., Yu, K., Pandolfi, J.M., 2009. High-precision U-series dating of very young cyclone-transported coral reef blocks from Heron and Wistari reefs, southern Great Barrier Reef, Australia. Quaternary International 195, 122–127.

Please cite this article as: Lau, A.Y.A., et al., Boulder emplacement and remobilisation by cyclone and submarine landslide tsunami waves near Suva City, Fiji, Sedimentary Geology (2017), https://doi.org/10.1016/j.sedgeo.2017.12.017